# Variable-stiffness composites optimisation under multiple design requirements and loads

Michele Iacopo Izzi, Marco Montemurro *, Anita Catapano

*Arts et Métiers Institute of Technology, Université de Bordeaux, CNRS, INRA, Bordeaux INP, HESAM Université, I2M UMR 5295, F-33405, Talence, France*

*Keywords:*
Variable-stiffness composite
Multi-level optimisation
Polar method
B-spline
Buckling
Strength
Manufacturing constraints

A B S T R A C T

The aim of this paper is twofold. On the one hand, it presents a methodology for the deterministic optimisation of a general class of variable-stiffness composite (VSC) structures, including a solution obtained by using laminæ with a curvilinear fibres-path and variable-thickness, by considering different design requirements under multiple load cases. The considered framework is the multi-level design methodology based on the polar parameters (PPs) to describe the macroscopic behaviour of the VSC structure. Particularly, only the first-level problem is addressed in this work: the design variables are, thus, the PPs and the thickness of the VSC laminate, whose spatial distribution is described via basis spline (B-spline) surfaces. The goal is to minimise the mass of the VSC structure subject to design requirements on feasibility, strength, first buckling load and maximum curvature of the fibres-path. This latter is formulated as an equivalent (conservative) constraint in the PPs space, regardless of the fibres-path within each lamina. Moreover, a general formulation of the gradient of the requirements related to buckling load and strength is proposed, which takes advantage from the main properties of B-spline entities and PPs. On the other hand, this paper aims to propose a new benchmark problem that is representative of a panel belonging to the fuselage of a standard civil aircraft subjected to multiple loading conditions. To this end, a wide campaign of numerical tests has been performed by considering a sensitivity analysis of the optimised solution to: (a) the integer parameters involved in the definition of the B-spline entities describing the distribution of the PPs and, possibly, of the thickness, (b) the type of VSC structure, (c) the type of deterministic optimisation algorithm. The results can be used as a database to assess the effectiveness of different design strategies against the optimised solutions presented in this paper.

## 1. Introduction

Modern manufacturing processes, like fused filament fabrication (FFF) technology combined with continuous filament fabrication (CFF) one [1–4], or automated fibre placement (AFP) [5–9] and continuous tow shearing (CTS) [10] technologies, allow fabricating variable-stiffness composite laminates (VSCLs) with uniform thickness wherein the filament (in the case of the FFF+CFF process) or the tow (in the case of the AFP and CTS technologies) is steered along a curvilinear (possibly optimised) path within each lamina. This class of VSCLs is often referred to as variable-angle tow laminates.

An alternative way of obtaining VSCLs consists of using a straight-fibres format within each ply and by varying the thickness (i.e., the number of layers) of each "laminate-patch" composing the structure. However, this operation cannot be performed without considering the so-called blending (or ply drop) requirement [11–13]. This requirement deals with the continuity of ply orientation angles between adjacent composite laminates having different thickness. Of course, a hybrid (more general) solution exploiting the main features of the two above classes can be obtained by using variable-angle tow laminates within composite structures made of patches of different thickness by considering tows/filaments and plies drops among adjacent laminates. This type of VSCLs can be obtained, for instance, by using recent additive manufacturing processes for composite materials, like the FFF+CFF technology.

Nevertheless, the potential behind additive manufacturing processes for composite materials is, today, still not fully exploited. By properly tuning the process parameters one can imagine to fabricate a more general class of composite structures, wherein the filaments can be steered along a curvilinear path inside layers of variable thickness. Possibly, the fibres volume fraction of each layer can be kept (almost) constant by varying the density of the filaments according to the thickness

* Corresponding author.
*E-mail address:* marco.montemurro@ensam.eu (M. Montemurro).

https://doi.org/10.1016/j.ijmecsci.2023.108537

variation. This type of VSCLs will be referred to as *variable-thickness* VSCLs in the following of the paper.

This work will focus, thus, on this general class of VSCLs, which are characterised by a continuous variation of the fibres-path and of the thickness of each lamina without considering a discontinuous ply drop between the regions characterised by different thickness. Therefore, the development of an efficient, robust and reliable design methodology accounting for different design requirements related to variable-thickness VSCLs is of paramount importance. Of course, the design of variable-thickness VSCLs, as the one of classical VSCLs, is an intrinsically multi-scale problem that can be dealt with through two different approaches [14,15].

The first one is commonly referred to as *direct approach* and consists in taking, as design variables, the parameters describing the fibres-path within each lamina [16–38]. Without any ambition of exhaustiveness, one can cite the work by Gürdal and Olmedo [18] wherein a linear function is used to describe the local fibre orientation angle: this parametrisation was later used by Alhajahmad et al. [19] to maximise the failure load of a VSCL with a cut-out made of a 16-ply symmetric balanced stacking sequence with only two independent local orientation angles of the type $[\pm\theta_1, \pm\theta_2]_{2S}$ (the optimisation was performed through a metaheuristic algorithm). Huang and Hatfka [20] made use of piece-wise bi-linear interpolation to describe the fibres-path within each ply with the aim of maximising the failure load of a plate with a cut-out subjected to a uni-axial tensile load, whilst Nagendra et al. [21] and Cao et al. [23] employed non-uniform rational basis spline curves to describe the fibres-path of the lamina. Recently, an interesting approach has been proposed by Tian et al. [22] wherein the fibres-path of the generic ply is described via a divergence-free vector field locally tangent to the fibres direction. More recent approaches make use of multi-fidelity surrogate models (i.e. surrogate models obtained by combining the results of low-fidelity and high-fidelity numerical models of the variable stiffness composite structure) to try to speed up the optimisation process [39–45].

Regardless of the adopted modelling strategy, the main limitations of the direct approach are essentially four: (i) the number of design variables is proportional to the number of layers, thus, it becomes considerably high for thick VSCLs; (ii) the number of layers cannot be included within the vector of design variables in the framework of a deterministic optimisation process because it is not a continuous variable; (iii) the structural responses depend upon combinations of trigonometric functions (up to the power four) of the local fibres orientation, thus, the related optimisation problem is a non-convex multi-modal problem (i.e., a problem characterised by a huge number of equivalent local minima); (iv) to find a solution in a reasonable time, researchers systematically introduce simplifying assumptions on the nature of the stacking sequence, e.g., the use of symmetric stacks to ensure a zero membrane/bending coupling stiffness matrix or the use of balanced stacks to get an orthotropic membrane stiffness matrix (although the bending one remains anisotropic).

The second approach, which has been introduced to overcome the limitations of the direct approach, is often referred to as *multi-level approach*. In the framework of the multi-level approach, the design problem of a VSCL is articulated in two (or more) sub-problems focusing on different scales. In the first-level problem (FLP), which is formulated at the macroscopic scale, the VSCL is represented as an equivalent homogeneous anisotropic single-layer plate whose behaviour is usually described either in the lamination parameters (LPs) space [15,46–52] or in the polar parameters (PPs) space [53–58]. It is noteworthy that the representation of the anisotropy based on the PPs is characterised by, at least, two advantages when compared to the representation based on LPs [53–55]. Firstly, the polar formalism has been generalised to the case of higher-order theories [59–61], thus it can be applied to the design of moderately thick to thick VSCLs. Secondly, it allows expressing a general $n$-rank plane tensor by means of a set of invariants related to its elastic symmetries, thus optimising the PPs fields allows to determine, locally, the best elastic symmetry type and its best orientation. Finally, it is noteworthy that, thanks to the polar formalism and to the original problem formulation (and the related numerical strategies) presented in [57,58], it has been possible to obtain optimised configurations outperforming those resulting from the use of the representation based on LPs on the same benchmark structures [46,47]. Therefore, the representation of the anisotropy based on the PPs will be employed also in this paper. By extending the approach presented in [55] to the most general case of a variable-thickness VSCL, the design variables of the FLP are the parameters tuning the field functions used to describe the distribution of the PPs and the thickness over the structure. It is noteworthy that the manufacturing constraints must be translated into equivalent (possibly conservative) constraints in terms of PPs and overall thickness of the structure.

Once a proper formulation of all mechanical and technological design requirements in the PPs space has been derived and (at least) one solution has been found for the FLP, it is possible to consider the second step of the multi-level procedure that focuses on the mesoscopic scale: the stacking sequence recovery phase, also called second-level problem (SLP). Particularly, the goal of this phase, is the determination of, at least, one optimum stack matching, locally, the optimised distribution of the PPs and of the thickness resulting from the resolution of the FLP. Generally, the recovery of a suitable stacking sequence is formulated as an unconstrained optimisation problem wherein the design variables are the parameters describing the fibres-path within each lamina. A further advantage of the approach based on PPs is that the stack recovery phase can be formulated in a very general way, i.e., without introducing hypotheses neither on the nature of the stacking sequence nor on the shape of the fibres-path [53,54,56].

Either the representation based on LPs or the one based on the PPs have been extensively used to deal with the optimisation of VSCLs including design requirements on stiffness [14,15,55], buckling load [46,48,57] and failure load [47,58]. The works dealing with the minimisation of the compliance of VSCLs are, undoubtedly, the most frequent ones available in the literature [14,15,55].

Regarding the design requirement related to the first buckling load, one can cite the works by Ijsselmuiden et al. [48] dealing with the maximisation of the first buckling load of a VSCL by considering a conservative approximation method wherein the buckling load is expressed as a linear combination of the in-plane and bending stiffness matrix terms in the space of the LPs. Wu et al. [46] made use of a deterministic algorithm to maximise the first buckling load of a VSCL subject to feasibility constraints on the LPs, whose distribution over the structure is represented through basis spline (B-spline) surfaces. Recently, Fiordilino et al. [57] proposed an alternative formulation of the problem of maximising the first buckling load of a VSCL subject to feasibility constraint on PPs (whose distribution over the structure is represented via B-spline entities), without introducing simplifying hypotheses on the behaviour of the stack: the results obtained by formulating the problem in the PPs space outperform those found by Wu et al. [46] and provide a clear evidence about the advantages related to the use of PPs in the framework of multi-level design strategies for VSCLs.

As far as the requirement on the failure load is concerned, it is noteworthy to mention the work by Ijsselmuiden et al. [49] wherein a conservative failure envelope in the LPs space is proposed. Such formulation has been subsequently employed by Khani et al. [47] to maximise the failure load of a VSCL square plate with a circular hole withstanding tensile loads subject to feasibility constraint on the LPs. An alternative formulation has been recently presented by Izzi et al. [58] wherein the problem of maximising the failure load of the VSCL has been formulated in the PPs space by using the unified formulation of different laminate-level failure criteria proposed by Catapano and Montemurro [62]. Thanks to an efficient change of variables remapping the feasibility constraints on the PPs over the unit square and to an efficient numerical framework exploiting the properties of B-spline

entities (used to represent the variation of the PPs over the structure), it has been possible to find optimised configuration characterised by failure load considerably higher than those characterising the optimised solutions presented by Khani et al. [47].

In the light of the above (non-exhaustive) literature survey, one can infer that most of the research works available in the literature focuses on the optimisation of VSCLs without considering variable thickness solutions and by including only one design requirement of mechanical nature (among stiffness, failure load and first buckling load) in the problem formulation as objective/constraint function. Moreover, in most of the considered research studies, only single loading conditions are considered. To go beyond these limitations, the aim of the present work is twofold. Firstly, since this work is focused only on the FLP of the multi-scale two-level optimisation strategy (MS2LOS) for VSCLs based on PPs and B-spline entities [55], which must be solved via a deterministic algorithm, a general problem formulation including design requirements related to mass, to first buckling load, to failure load, to feasibility conditions and to manufacturing constraint on the maximum admissible curvature of the filament/tow (reformulated in the PPs space) of variable-thickness VSCLs is presented. In this context, the first original contribution of this paper is represented by a formulation of the gradient of the buckling load more general than that presented by Fiordilino et al. [57], which can be used for general shell elements of whatever shape. Regarding the formulation of the failure load requirement and of the manufacturing constraint (and of the related gradient expressions), the general formulation presented by Izzi et al. [58] is employed in this work.

Secondly, this work aims to propose a benchmark problem, representative of a fuselage panel with a porthole withstanding multiple loading conditions, whose results can be exploited by other researchers in the field of composite structures to check/validate the accuracy of alternative optimisation strategies (belonging to the family of multi-level approaches) to design VSCLs or to propose better design methodologies. To the best of the authors' knowledge, a general benchmark problem for VSCLs considering multiple loading conditions and including conflicting design requirements, such as those mentioned above, in the problem formulation has never been proposed in the literature. In order to provide an exhaustive analysis of the proposed benchmark problem, an extensive campaign of numerical analyses has been performed on this benchmark structure by considering different classes of VSCLs (with both uniform and variable thickness) and by investigating the influence of the integer parameters involved in the definition of the B-spline entities (used to describe the distribution of the PPs and of the thickness over the structure) on the optimised solutions. A further sensitivity analysis has been conducted to investigate the influence of two different deterministic optimisation algorithms, i.e., the Sequential Least-Squares Quadratic Programming (SLSQP) and the Globally Convergent Method of Moving Asymptotes (GCMMA) algorithms, on the optimised solutions: the results of this analysis allows inferring useful remarks and guidelines on their use in relation with the non-convex nature of the design problem at hand and the performances of the local minimisers.

The paper is organised as follows. The definition of the benchmark structure with the related load cases and design requirements is presented in Section 2. The mathematical formulation of the FLP is detailed in Section 3 by considering a deterministic optimisation framework. The finite element (FE) model of the structure is presented in Section 4, whilst the numerical results are presented and discussed in Section 5. Finally, Section 6 provides meaningful conclusions and prospects.

*Notation.* Upper-case bold letters and symbols are used to indicate matrices, while lower-case bold letters and symbols indicate vectors, which are to be intended as column ones.

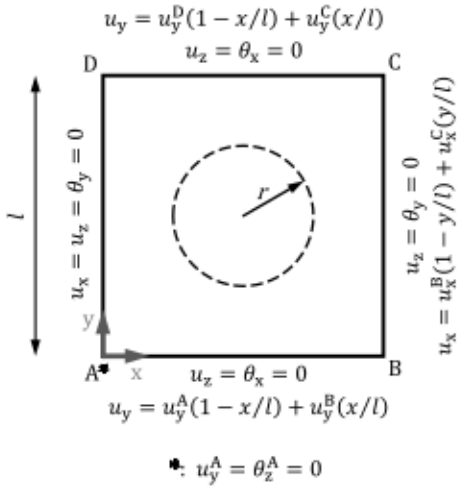


**Fig. 1.** Geometry and displacement boundary conditions of the benchmark structure.

## 2. Definition of the benchmark structure

To show the effectiveness of the MS2LOS for designing VSCLs, a meaningful benchmark problem is defined: the least-weight design of a square VSC plate of side $l$ with a central circular plastic porthole of radius $r$ (shown in Fig. 1), subject to multiple design requirements. Such requirements include a constraint on the first buckling load, a constraint on the failure load and constraints on the manufacturability of the structure. This structure represents a simplified "flat model" of a panel extracted from a stiffened vessel of radius $R$ having a plugged opening and withstanding pressurisation and other external loads. Of course, this structure can be considered as a representative of an industrial application when the radius of curvature assumes a sufficiently high value (which is the case of the panels belonging to the fuselage of standard civil aircraft).

The composite plate constitutes the design region (DR) of the structure and is made of unidirectional AS4/3501-6 carbon/epoxy pre-preg tows. The material properties of the constitutive pre-preg tow are reported in Table 1 (for the meaning of the polar parameters listed in this table the reader is addressed to [58]). The porthole constitutes the non-design region (NDR) of the structure and is a plate of uniform thickness $t_{ph}$ made of isotropic acrylic plastic whose properties are reported in Table 2.

The *reference solution* (RSol) is defined as the structure having a homogeneous isotropic DR of uniform thickness $t_{RSol}$.

The structure is constrained on its outer edges as shown in Fig. 1. Part of these constraints ensures that the outer edges of the structure remain straight while withstanding external loads. The plate and the porthole are considered perfectly bonded to each other on the inner common edge, without overlap. Two load cases (LCs) are considered and four basic loading conditions are identified. By referring to Fig. 2, these loading conditions are:

**Uni-axial compression.** A distribution of compressive forces per unit length $\bar{n}_{x,C}(y)$ is applied along the x axis on edge BC whose resultant is $F_C$ (Fig. 2(a)).

**In-plane bending.** A distribution of forces per unit length $\bar{n}_{x,M}(y)$ is applied on edge BC along the $x$ axis, whose resultant is the bending moment $M_B$ around the $z$ axis (Fig. 2(b)).

**In-plane shear.** A uniform distribution of in-plane shear forces per unit length $\bar{n}_{xy}$ is applied on all edges (Fig. 2(c)).

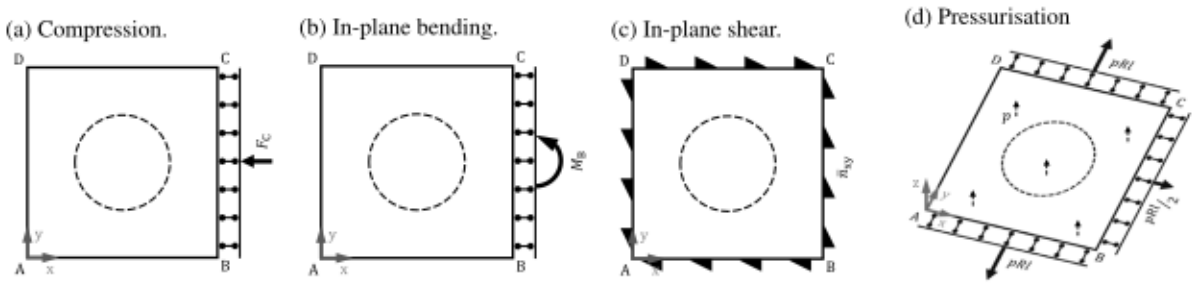


**Fig. 2.** Basic loading conditions acting on the benchmark structure and used to define the two considered load cases.

**Table 1**
Material properties of the unidirectional AS4/3501-6 carbon/epoxy tow used in the design region of the benchmark structure [47,58,63].

| Technical constants | | Polar parameters of $\mathbf{Q}^{n}$ [a] | | Polar parameters of $\mathbf{Q}^{out}$ [b] | |
|---|---|---|---|---|---|
| $E_1$ [MPa] | 142000 | $T_0^{Q_{in}}$ [MPa] | 22040 | $T^{Q_{out}}$ [MPa] | 5272 |
| $E_2$ [MPa] | 10300 | $T_1^{Q_{in}}$ [MPa] | 19838 | $R^{Q_{out}}$ [MPa] | 1928 |
| $G_{12}$ [MPa] | 7200 | $R_0^{Q_{in}}$ [MPa] | 14840 | $\Phi^{Q_{out}}$ [rad] | $\pi/2$ |
| $\nu_{12}$ | 0.27 | $R_1^{Q_{in}}$ [MPa] | 16550 | | |
| $\nu_{23}$ | 0.54 | $\Phi_0^{Q_{in}}$ [rad] | 0 | | |
| | | $\Phi_1^{Q_{in}}$ [rad] | 0 | | |
| **Engineering strengths** | | **Pol. par. of $\mathbf{G}^{n}$ [c]** | | **Pol. par. of $\mathbf{G}^{out}$ [d] and $\mathbf{g}^{in}$ [e]** | |
| $X$ [MPa] | 2280 | $T_0^{G_{in}}$ [MPa] | 7077 | $T^{G_{out}}$ [MPa] | 8637 |
| $X'$ [MPa] | 1440 | $T_1^{G_{in}}$ [MPa] | 1312 | $R^{G_{out}}$ [MPa] | 1647 |
| $Y = Z$ [MPa] | 57 | $R_0^{G_{in}}$ [MPa] | 3206 | $\Phi^{G_{out}}$ [rad] | $\pi/2$ |
| $Y' = Z'$ [MPa] | 228 | $R_1^{G_{in}}$ [MPa] | 405 | $T^{g_{in}}$ [MPa] | 68 |
| $Q$ [MPa] | 40 | $\Phi_0^{G_{in}}$ [rad] | $\pi/4$ | $R^{g_{in}}$ [MPa] | 68 |
| $R = S$ [MPa] | 71 | $\Phi_1^{G_{in}}$ [rad] | $\pi/2$ | $\Phi^{g_{in}}$ [rad] | $\pi/2$ |
| Density | | $\rho$ [g/cm$^3$] | 1.58 | | |

[a] In-plane reduced stiffness matrix of the ply.
[b] Out-of-plane shear stiffness matrix of the ply.
[c] In-plane strength matrix of the ply.
[d] Out-of-plane strength matrix of the ply.
[e] In-plane strength vector of the ply.

**Table 2**
Material properties of the acrylic plastic constituting the porthole.

| Property | Sym. | Value |
|---|---|---|
| Young's modulus [MPa] | $E$ | 3210 |
| Poisson's ratio [–] | $\nu$ | 0.38 |

**Pressurisation.** A uniform pressure $p$ is applied on the whole structure, completed by the corresponding membrane tensile loads (in analogy to the loads of a pressurised vessel of radius $R$ whose longitudinal axis is perpendicular to the x axis of the structure).

LC1 is the sum of the first three basic loading conditions above and is applied for a more conservative evaluation of the buckling load. Indeed, the last loading condition is excluded from LC1 because the pressurisation and its related tensile membrane loads increase the buckling load of the structure. LC2 is applied for the evaluation of the failure load of the structure and consists of the sum of all four aforementioned basic loading conditions. $F_C$, $M_B$, $\bar{n}_{xy}$, and $p$ have been set to the minimum values ensuring that RSol withstands LC1 and LC2 without buckling or failure, respectively. Moreover, they have been set in such a way that the corresponding basic load conditions are equally critical (i.e., same factor of safety) with respect to failure when applied separately on RSol.[1] The values of the applied forces and of the geometric parameters of the structure are reported in Table 3.

[1] In this way, RSol is, by construction, the least-weight no-buckling and no-failure uniform-thickness homogeneous isotropic composite solution for the considered design case.

**Table 3**
Geometrical characteristics of the benchmark structure, and values of the loads acting on it.

| Parameter | Sym. | Value |
|---|---|---|
| Side length [mm] | $l$ | 400 |
| Porthole radius [mm] | $r$ | 100 |
| Porthole thickness [mm] | $t_{ph}$ | 10 |
| Reference thickness [mm] | $t_{RSol}$ | 4.6 |
| Vessel radius [mm] | $R$ | 2000 |
| Resultant compressive force [N] | $F_C$ | $1.498 \cdot 10^5$ |
| Resultant bending moment [N mm] | $M_B$ | $1.779 \cdot 10^7$ |
| Shear load per unit length [N/mm] | $\bar{n}_{xy}$ | 80.90 |
| Pressure [MPa] | $p$ | 0.098 |

As discussed in Section 3, the design problem is formulated as a constrained non-linear programming problem (CNLPP): the goal is the minimisation of the mass of the structure subject to constraints on its first buckling load and failure load (which must be greater than or equal to those of RSol) and a constraint on the maximum curvature of the tows composing its composite part. The structure is made of a point-wise fully orthotropic, quasi-homogeneous VSCL, i.e., a VSCL having the same orthotropic behaviour in terms of normalised membrane and bending stiffness matrices with a zero membrane/bending coupling stiffness matrix [59]. Specifically, three sub-classes of VSCLs, previously introduced by the authors [58], are considered:

**C1** Uniform-Thickness VSCLs with *Variable Orthotropy Direction* (UT-DVO), but uniform anisotropic moduli, i.e., this class of VSCLs is characterised by the same type of orthotropy at each point of the structure, except the orientation of the main axis of orthotropy that varies point-wise.

**C2** Uniform-Thickness VSCLs with a *Fully Variable Orthotropy* (UT-FVO), i.e., the orthotropy type and the orientation of the main axis of orthotropy vary at each point of the design domain for this class of VSCLs.

**C3** Variable-Thickness VSCLs with a Fully Variable Orthotropy (VT-FVO).

In this context, the adjectives uniform and variable refer to the spatial variation of the properties over the laminate. The application of the requirement on the maximum tow curvature is currently limited to VSCLs belonging to sub-class C1 because, up to now, an equivalent formulation of this requirement in the PPs space has been determined only for this class of VSCLs [54,58].

Regarding the behaviour and the modelling of the benchmark structure, the following hypotheses apply:

**H1** The behaviour of the material constituting both DR and NDR is linear elastic and the hypothesis of small perturbations (i.e., small generalised displacements and strain) is assumed for FE analyses.

**H2** The macroscopic behaviour of the VSCL is described in the framework of the first-order shear deformation theory (FSDT).

**H3** The plastic porthole does not fail under considered load cases.

**H4** Regarding VSCLs-C3, the spatial variation of thickness is considered continuous and symmetric with respect to the laminate middle plane.

**H5** The DR is composed of an "ideal material", i.e., without the presence of defects due to the manufacturing process of the VSCL, like gaps and overlaps among adjacent tows.

Of course, these last two hypotheses correspond to solutions that are not manufacturable with current processes. These solutions can be interpreted as the theoretical limit achievable by using increasingly thinner and narrower tows in the AFP manufacturing process, or with the evolution of modern additive manufacturing technologies for composite materials [3].

## 3. Mathematical formulation of the first-level problem

The main features of the FLP of the MS2LOS for the optimum design of VSCLs are described in this section by putting the accent on the new contributions introduced in this work. More details on the MS2LOS for designing VSCLs can be found in [55,57,58].

The macroscopic response of the VSCL is described in the framework of the FSDT, whose constitutive equation (expressed in the local frame $\Gamma_e = \{O; x_e, y_e, z_e\}$) reads:

$$\mathbf{r} = \mathbf{K}_{\text{Lam}}\boldsymbol{\varepsilon}, \tag{1}$$

where $\mathbf{r}$ and $\boldsymbol{\varepsilon}$ are the vectors of the generalised forces per unit length and the strains of the laminate middle plane, respectively, whilst $\mathbf{K}_{\text{Lam}}$ is the laminate stiffness matrix (Voigt's notation). The expression of the above vectors and matrix is:

$$\mathbf{r} := \begin{Bmatrix} \mathbf{n} \\ \mathbf{m} \\ \mathbf{q} \end{Bmatrix}, \quad \mathbf{K}_{\text{Lam}} := \begin{bmatrix} \mathbf{A} & \mathbf{B} & \mathbf{0} \\ & \mathbf{D} & \mathbf{0} \\ \text{sym} & & \mathbf{H} \end{bmatrix}, \quad \boldsymbol{\varepsilon} := \begin{Bmatrix} \boldsymbol{\varepsilon}_0 \\ \boldsymbol{\chi}_0 \\ \boldsymbol{\gamma}_0 \end{Bmatrix}. \tag{2}$$

In Eq. (2), $\mathbf{A}$, $\mathbf{B}$ and $\mathbf{D}$ are the membrane, membrane/bending coupling and bending stiffness matrices of the laminate, $\mathbf{H}$ is the out-of-plane shear stiffness matrix, $\mathbf{n}$, $\mathbf{m}$ and $\mathbf{q}$ are the vectors of membrane forces, bending moments and shear forces per unit length, respectively, whilst $\boldsymbol{\varepsilon}_0$, $\boldsymbol{\chi}_0$ and $\boldsymbol{\gamma}_0$ are the vectors of in-plane strains, curvatures and out-of-plane shear strains of the laminate middle plane, respectively.

In the following of this section, the normalised stiffness matrices are introduced to analyse the elastic response of the VSCL. They are defined as:

$$\mathbf{A}^* := \frac{1}{t}\mathbf{A}, \quad \mathbf{B}^* := \frac{2}{t^2}\mathbf{B}, \quad \mathbf{D}^* := \frac{12}{t^3}\mathbf{D}, \quad \mathbf{H}^* := \frac{1}{t}\mathbf{H}, \tag{3}$$

where $t$ is the total thickness of the laminate.

### 3.1. Design variables

As discussed by Montemurro and Catapano [55], the macroscopic behaviour of a quasi-homogeneous, orthotropic VSCL is uniquely described through four quantities: the thickness of the VSCL $t$ and the three PPs $R_{0K}^{\text{A}^*}$, $R_1^{\text{A}^*}$ and $\Phi_1^{\text{A}^*}$. When dealing with the FLP formulation, it is useful to introduce the following dimensionless quantities:

$$\tau := \frac{t}{t_{\text{RSol}}}, \quad \rho_{0K} := \frac{R_{0K}^{\text{A}^*}}{R_0^{\text{Q}_{\text{in}}}}, \quad \rho_1 := \frac{R_1^{\text{A}^*}}{R_1^{\text{Q}_{\text{in}}}}, \quad \phi_1 := \frac{\Phi_1^{\text{A}^*}}{\pi/2}, \tag{4}$$

As widely discussed by Vannucci [64], the optimal value of the PPs constituting the solution of the FLP must correspond to a feasible stacking sequence to be determined as a solution of the subsequent SLP. To this end, suitable feasibility constraints must be integrated in the formulation of the FLP. However, as discussed by Picchi Scardaoni and Montemurro [65], the feasibility constraints proposed by Vannucci [64] constitute just the convex-hull of the true feasibility domain. Indeed, as explained by Picchi Scardaoni and Montemurro [65], the convex approximation of the true feasibility domain can be considered in the FLP formulation only if the laminate is made of a sufficiently high number of laminæ (theoretically an infinite number) with the orientation angles of the plies taking value in a sufficiently big and scattered set. To avoid introducing the optimisation constraints describing the convex-hull of the feasibility domain presented by Vannucci [64] into the FLP formulation, the following variable change, recently introduced by the authors [58], is used:

$$(\alpha_0, \alpha_1) := \left(\frac{\rho_{0K} - 1}{2(\rho_1^2 - 1)}, \rho_1\right), \tag{5}$$

whose converse relation is

$$(\rho_{0K}, \rho_1) = (1 + 2\alpha_0(\alpha_1^2 - 1), \alpha_1). \tag{6}$$

This variable change consists of remapping the convex-hull of the feasibility region of the PPs space over a unit square domain $[0,1] \times [0,1]$: accordingly, all combinations of $\alpha_0$ and $\alpha_1$ satisfy the feasibility conditions presented by Vannucci [64].

In agreement with Eqs. (4) and (5), four independent fields are needed to describe the elastic response of the VSCL at the macroscopic scale, i.e., $\tau$, $\alpha_0$, $\alpha_1$, $\phi_1$. Each field can be either uniform or variable over the laminate, depending on the considered VSCL sub-class (see Section 2). Particularly, VSCLs belonging to sub-class C1 are characterised by non-uniform distribution of $\phi_1$ and uniform distribution of $\tau$, $\alpha_0$, and $\alpha_1$. When VSCLs belonging to sub-class C2 are considered, $\alpha_0$, $\alpha_1$, and $\phi_1$ are non-uniform fields, whilst $\tau$ is uniform over the DR. Lastly, for VSCLs belonging to sub-class C3 all fields are non-uniform. The generic field $\xi$ is described through a B-spline scalar function [55,57,58]:

$$\xi(u_1, u_2) = \sum_{i_1=0}^{n_1}\sum_{i_2=0}^{n_2} N_{i_1,p_1}(u_1) N_{i_2,p_2}(u_2) \xi^{(i_1,i_2)}, \quad \text{with } \xi = \tau, \alpha_0, \alpha_1, \phi_1, \tag{7}$$

where $\xi^{(i_1,i_2)}$ is the value of the field at the generic control point (CP), whereas $N_{i_1,p_1}(u_1)$ and $N_{i_2,p_2}(u_2)$ are the Bernstein's polynomials of degree $p_1$ and $p_2$ computed at parametric coordinates $u_1$ and $u_2$, which are defined as:

$$(u_1, u_2) := \left(\frac{x}{l}, \frac{y}{l}\right), \quad u_1, u_2 \in [0,1], \tag{8}$$

where $x$ and $y$ are the Cartesian coordinates, as illustrated in Fig. 1. In agreement with the classical theory of B-spline entities [66], $n_d + 1$ CPs are needed along the $d$-th parametric direction, for a total number of CPs equal to $N_{\text{CP}} = (n_1 + 1) \times (n_2 + 1)$. Note that Bernstein's polynomials introduced in Eq. (7) are defined span-wise through the so-called *knot vectors*:

$$\mathbf{v}^{(d)\text{T}} := \left\{\underbrace{0, \dots, 0}_{p_d}, v_{p_d}^d, \dots, v_{n_d+1}^d, \underbrace{1, \dots, 1}_{p_d}\right\}, \quad \text{with } d = 1, 2. \tag{9}$$

As already done in previous works [55,57,58], the inner components of the knot-vectors, the number of CPs and the degree of the Bernstein's polynomials along each parametric direction are set by the user before the optimisation process and are not considered among the design variables of the FLP. Particularly, the inner terms of the knot vectors are evenly distributed in the interval $]0,1[$. More details on B-spline entities are available in the book by Piegl and Tiller [66].

In the light of the above remarks, only the value of the generic field at each CP, i.e., $\xi^{(i_1,i_2)}$, is integrated in the vector of design variables. Accordingly, the overall number of design variables characterising the VSCL depends upon the sub-class to which it belongs, as listed in Table 4. In the most general case, i.e., when $\tau$, $\alpha_0$, $\alpha_1$ and $\phi_1$ are non-uniform fields, the total number of design variables is $4 \times N_{\text{CP}}$. They

**Table 4**
Number of design variables for each sub-class of variable-stiffness composite laminates considered.

| | $\tau$ | $\alpha_0$ | $\alpha_1$ | $\phi_1$ | Total |
|---|---|---|---|---|---|
| C1 | 1 | 1 | 1 | $N_{CP}$ | $3 + N_{CP}$ |
| C2 | 1 | $N_{CP}$ | $N_{CP}$ | $N_{CP}$ | $1 + 3 \times N_{CP}$ |
| C3 | $N_{CP}$ | $N_{CP}$ | $N_{CP}$ | $N_{CP}$ | $4 \times N_{CP}$ |

are collected in the vector $\mathbf{x}$ as:

$$\mathbf{x}^{\mathrm{T}} := \left\{ \tau^{(0,0)}, \dots, \tau^{(n_1,n_2)}, \alpha_0^{(0,0)}, \dots, \alpha_0^{(n_1,n_2)}, \alpha_1^{(0,0)}, \dots, \alpha_1^{(n_1,n_2)}, \phi_1^{(0,0)}, \dots, \phi_1^{(n_1,n_2)} \right\}. \tag{10}$$

### 3.2. Structural responses and their gradients

As discussed in Section 2, four types of requirements are involved in the formulation of the FLP considered in this work. Specifically, design requirements are formulated on: (a) the mass, (b) the first buckling load, (c) the failure load, (d) the curvature of the tows. To solve the FLP by means of a deterministic algorithm, the formal derivation of the expression of the response function and of its gradient are needed for each requirement. The above design requirements are computed as results of both linear static and eigenvalue buckling FE analyses. Regarding static analyses, the equilibrium equation (expressed within the global frame of the structure $\mathcal{F} = \{O; x, y, z\}$) reads:

$$\mathbf{K}\mathbf{u} = \mathbf{f} = \lambda \mathbf{f}_{\mathrm{Ref}}. \tag{11}$$

where $\mathbf{K}$ is the global stiffness matrix of the structure, $\mathbf{u}$ is the vector of the degrees of freedom (DOFs) collecting both unknown and imposed DOFs, $\mathbf{f}$ is the vector of generalised external nodal forces defined as the product of the load factor $\lambda$ and the reference load vector $\mathbf{f}_{\mathrm{Ref}}$ (which can either be the one related to LC1 or the one related to LC2, depending on the assessed requirement). Eq. (11) can be arranged such that the unknown DOFs, indicated with a subscript F, are separated from imposed DOFs, identified by a subscript D:

$$\underbrace{\begin{bmatrix} \mathbf{K}^*_{\mathbf{FF}} & \mathbf{K}^*_{\mathbf{FD}} \\ \mathbf{K}^*_{\mathbf{DF}} & \mathbf{K}^*_{\mathbf{DD}} \end{bmatrix}}_{\mathbf{K}^*} \underbrace{\begin{Bmatrix} \mathbf{u}^*_{\mathrm{F}} \\ \mathbf{u}^*_{\mathrm{D}} \end{Bmatrix}}_{\mathbf{u}^*} = \lambda \underbrace{\begin{Bmatrix} \mathbf{f}^*_{\mathrm{Ref,F}} \\ \mathbf{f}^*_{\mathrm{Ref,D}} \end{Bmatrix}}_{\mathbf{f}^*_{\mathrm{Ref}}}, \tag{12}$$

where the superscript $*$ means *reordered* and, of course, $\mathbf{K}^*_{\mathbf{DF}} = \mathbf{K}^{*\mathrm{T}}_{\mathbf{FD}}$.

The eigenvalue buckling problem in the FE framework is stated as

$$\left(\mathbf{K} + \lambda_b \mathbf{S}_{\mathrm{Ref}}\right) \mathbf{u}_b = \mathbf{0} \;\text{ with }\; \mathbf{u}_b \neq \mathbf{0}, \tag{13}$$

where $\mathbf{S}_{\mathrm{Ref}}$ is the stress stiffening matrix, which depends on the geometric characteristics of the structure and on the stress field associated to the static problem of Eq. (11) when $\lambda = 1$ and the suited Ref LC is applied (i.e., LC1 in the considered design case), $\lambda_b$ is the $b$th eigenvalue of the system (i.e., buckling load factor of the structure), and $\mathbf{u}_b$ is the $b$th eigenvector (i.e., buckling mode) associated to $\lambda_b$.

The expressions of the functions related to the mass, the failure load, and the tow curvature requirements have been derived in a previous work [58] and are hereafter recalled for the sake of clarity. As far as the buckling requirement is concerned, an expression of the response function and of its gradient more general than that presented by Fiordilino et al. [57] is derived and implemented in this work.

Structural responses related to maximum failure load and maximum tow curvature requirements are approximated through the $p$-Norm function that operates on an indexed set of values computed per-element ($q_e$) in the design region as follows:

$$pn(q_e) := \left( \sum_e q_e^p \right)^{1/p} \approx \max_e q_e, \tag{14}$$

where $p$ is the power of the norm, which is related to the accuracy of the approximation. Its value is chosen according to the formula [58]

$$p = \left\lceil \frac{\log N_e^{\mathrm{DR}}}{\log\left(1 + d_{\max}\right)} \right\rceil, \tag{15}$$

where $d_{\max}$ is the desired maximum relative difference between the value of the $p$-Norm and the value $q_{\max}$, and $N_e^{\mathrm{DR}}$ is the number of values upon which the $p$-Norm is computed, here equal to the number of elements belonging to the DR of the structure (Sections 2 and 4).

The derivative of the $p$-Norm operator with respect to the generic variable $\xi$ reads

$$\frac{\partial\left(pn(q_e)\right)}{\partial \xi} = \left(pn(q_e)\right)^{1-p} \sum_e \left( q_e^{p-1} \frac{\partial q_e}{\partial \xi} \right). \tag{16}$$

#### 3.2.1. Mass requirement

The design requirement related to the mass of the VSCL is defined as a relative difference between the mass of the DR of the structure, and a reference mass, here set equal to the mass of the composite part of the reference solution RSol:

$$f_{\mathrm{M}} := \frac{M_{\mathrm{DR}} - M_{\mathrm{Th}}}{M_{\mathrm{Th}}}, \tag{17}$$

with $M_{\mathrm{Th}} = M_{\mathrm{DR,RSol}}$. The mass of the VSCL is approximated as:

$$M_{\mathrm{DR}} \approx \rho \sum_{e \in S_{\mathrm{DR}}} \left( A_e t_e \right), \tag{18}$$

where $A_e$ is the area of the $e$th element and $t_e$ is the thickness evaluated at its centroid (obtained as $t_e = \tau_e\, t_{\mathrm{RSol}}$), whilst $S_{\mathrm{DR}}$ is the set collecting the ID of the elements belonging to the DR of the structure. The function $f_{\mathrm{M}}$ is linear with respect to the design variables $\xi^{(i_1,i_2)}$. A negative value of $f_{\mathrm{M}}$ means that the mass of the DR is lower than the reference value.

The partial derivative of $f_{\mathrm{M}}$ reads:

$$\frac{\partial f_{\mathrm{M}}}{\partial \xi^{(i_1,i_2)}} = \begin{cases} \dfrac{t_{\mathrm{RSol}}\rho}{M_{\mathrm{DR,RSol}}} \displaystyle\sum_{e \in LS_{i_1 i_2}} \left( A_e \frac{\partial \tau_e}{\partial \tau^{(i_1,i_2)}} \right) & \text{if } \xi = \tau, \\ 0 & \text{if } \xi \neq \tau, \end{cases} \tag{19}$$

where $LS_{i_1 i_2}$ indicates the discretised *local support* of the generic CP $(i_1, i_2)$, defined as:

$$LS_{i_1 i_2} := \left\{ e \in DR : (u_{1e}, u_{2e}) \in \left[ v_{i_1}^{(1)}, v_{i_1+p_1+1}^{(1)} \right[ \times \left[ v_{i_2}^{(2)}, v_{i_2+p_1+1}^{(2)} \right[ \right\}. \tag{20}$$

According to the *local support property* of B-spline basis functions [66], only the elements falling in the local support (or influence zone) of the CP $(i_1, i_2)$ are influenced by the variation of the generic design variable $\xi^{(i_1,i_2)}$. Of course, the size of the local support zone depends on the B-spline integer parameters. It is noteworthy that, according to Eq. (7), the partial derivative of the generic field $\xi$ computed at the centroid of the $e$th element ($\xi_e := \xi(u_{1e}, u_{2e})$) reads:

$$\frac{\partial \xi_e}{\partial \xi^{(i_1,i_2)}} = N_{i_1,p_1}(u_{1e})\; N_{i_2,p_2}(u_{2e}). \tag{21}$$

#### 3.2.2. Buckling requirement

For the application of the buckling requirement, the buckling factor of safety $\lambda_{\mathrm{B}}$ is introduced. It is defined as the minimum positive eigenvalue of Eq. (13), leading to instability of the structure:

$$\lambda_{\mathrm{B}} := \min_b(\lambda_b > 0). \tag{22}$$

The function related to the buckling requirement is simply defined as

$$f_{\mathrm{B}} := \frac{\lambda_{\mathrm{B,Th}} - \lambda_{\mathrm{B}}}{\lambda_{\mathrm{B,Th}}}, \tag{23}$$

where $\lambda_{\mathrm{B,Th}}$ is a threshold buckling load factor, here equal to $\lambda_{\mathrm{B,Th}} = \lambda_{\mathrm{B,RSol}}$, i.e., the buckling load factor of RSol withstanding a suited LC.

Clearly, a negative value of $f_B$ implies that the considered structure has a higher buckling load than RSol. For a VSCL submitted to given BCs, the gradient of $f_B$ can be obtained by solving the following system:

$$\begin{cases} \dfrac{\partial f_B}{\partial \xi^{(i_1,i_2)}} = -\dfrac{\lambda_B}{2U_B\lambda_{B,Th}}\left[\mathbf{u}_B^T\tilde{\boldsymbol{\psi}}_{B,i_1i_2} + \lambda_B\left(\sum_{e\in LS_{i_1i_2}} \dfrac{\partial\xi_e}{\partial\xi^{(i_1,i_2)}}\mathbf{s}_{B,e}^T\dfrac{\partial\mathbf{K}_{Lam,e}}{\partial\xi_e}\boldsymbol{\varepsilon}_{Ref,e} + \boldsymbol{\upsilon}_B^T\tilde{\boldsymbol{\psi}}_{Ref,i_1i_2}\right)\right], \\ \mathbf{K}_{FF}^*\ \boldsymbol{\upsilon}_{B,F}^* = -\boldsymbol{\psi}_{B,F}^*, \end{cases} \tag{24}$$

where:

- $U_B$ is the strain energy associated to the buckling mode deformation and it is defined as

$$U_B := \frac{1}{2}\mathbf{u}_B^T\mathbf{K}\mathbf{u}_B. \tag{25}$$

- $\tilde{\boldsymbol{\psi}}_{B,i_1i_2}$ and $\tilde{\boldsymbol{\psi}}_{Ref,i_1i_2}$ are two analogous fictitious force vectors defined as:

$$\tilde{\boldsymbol{\psi}}_{B,i_1i_2} := \sum_{e\in LS_{i_1i_2}}\left(\frac{\partial\xi_e}{\partial\xi^{(i_1,i_2)}}\cdot\int_{A_e}\mathfrak{L}_e^T\mathfrak{B}_e^T\frac{\partial\mathbf{K}_{Lam,e}}{\partial\xi_e}\mathfrak{B}_e\mathfrak{L}_e dS\right)\mathbf{u}_B, \tag{26}$$

and

$$\tilde{\boldsymbol{\psi}}_{Ref,i_1i_2} := \sum_{e\in LS_{i_1i_2}}\left(\frac{\partial\xi_e}{\partial\xi^{(i_1,i_2)}}\cdot\int_{A_e}\mathfrak{L}_e^T\mathfrak{B}_e^T\frac{\partial\mathbf{K}_{Lam,e}}{\partial\xi_e}\mathfrak{B}_e\mathfrak{L}_e dS\right)\mathbf{u}_{Ref}. \tag{27}$$

- $\mathbf{s}_{B,e}$ is an $8\times 1$ vector, whose components are defined as

$$\left(\mathbf{s}_{B,e}\right)_i := \mathbf{u}_B^T\mathfrak{L}_e^T\int_{A_e}\mathfrak{G}_e^T\mathbf{O}_i\mathfrak{G}_e dS\,\mathfrak{L}_e\mathbf{u}_B,\quad i=1,\dots,8. \tag{28}$$

- $\boldsymbol{\upsilon}_B^T := \left\{\boldsymbol{\upsilon}_{B,F}^{*\,T},\ \boldsymbol{\upsilon}_{B,D}^{*\,T}\right\}$ with $\boldsymbol{\upsilon}_{B,D}^* = \mathbf{0}$ is the auxiliary vector.
- $\boldsymbol{\psi}_B$ is defined as

$$\boldsymbol{\psi}_B := \sum_e \mathfrak{L}_e^T\mathfrak{B}_e^T\mathbf{K}_{Lam,e}\mathbf{s}_{B,e}. \tag{29}$$

Regarding the quantities $\boldsymbol{\varepsilon}_{Ref,e}$, $\mathfrak{B}_e$, $\mathfrak{L}_e$ and $\mathbf{u}_{Ref}$ appearing in Eqs. (24), (26) and (27), they are related as follows :

$$\boldsymbol{\varepsilon}_{Ref,e} = \mathfrak{B}_e\mathfrak{L}_e\mathbf{u}_{Ref}. \tag{30}$$

In Eq. (30), $\mathbf{u}_{Ref}$ is the solution of Eq. (11) with $\lambda = 1$, $\mathfrak{L}_e$ is the generalised connectivity matrix (including also the affine transformation aligning the element local frame $\Gamma_e$ to the global one $\Gamma$), which is defined as

$$\mathfrak{L}_e : \mathbf{u}\mapsto\mathbf{u}_e,\quad \mathbf{u}_e = \mathfrak{L}_e\mathbf{u}, \tag{31}$$

and $\mathfrak{B}_e$ is the matrix containing the partial derivatives of the shape functions of the element $e$ computed at its centroid, which is defined as

$$\mathfrak{B}_e : \mathbf{u}_e\mapsto\boldsymbol{\varepsilon}_e,\quad \boldsymbol{\varepsilon}_e = \mathfrak{B}_e\mathbf{u}_e. \tag{32}$$

The analytical expression of the laminate stiffness matrix $\mathbf{K}_{Lam}$ and its gradient can be found in [58], while the definition of $\mathfrak{G}_e$ and $\mathbf{O}_i$ appearing in Eq. (28) is given in Appendix A, where the proof of Eq. (24) is provided.

In the considered design case, the reference LC for the evaluation of the response function $f_B$ is LC1.

### 3.2.3. Failure load requirement

As far as the failure load requirement is concerned, the factor of safety $\lambda_F$ is introduced. It is defined as the least positive load factor bringing to the failure of the structure:

$$\lambda_F := \min_e \lambda_{F,e}, \tag{33}$$

where

$$\lambda_{F,e} := \left\{\lambda > 0 \mid F_e(\lambda) = F_{Th}\right\}. \tag{34}$$

In the above formula $F_e$ is the *laminate failure index* (LFI) [58,62] computed at the centroid of the generic element that reads

$$F_e := Q_e\lambda^2 + L_e\lambda, \tag{35}$$

where $Q_e$ and $L_e$ are defined as

$$Q_e := \boldsymbol{\epsilon}_{Ref,e}^T\frac{\mathbf{G}_{Lam,e}}{t}\boldsymbol{\epsilon}_{Ref,e},\quad L_e := \boldsymbol{\epsilon}_{Ref,e}^T\frac{\mathbf{g}_{Lam,e}}{t}. \tag{36}$$

In Eq. (36), $\mathbf{G}_{Lam,e}$ and $\mathbf{g}_{Lam,e}$ are the strength matrix and vector of the VSCL at the macroscopic scale, whose terms can be expressed as function of PPs $R_{0,K}^{A^*}$, $R_1^{A^*}$ and $\Phi_1^{A^*}$ and of the overall thickness $t$ of the VSCL [58,62]. As discussed by Izzi et al. [58], the value $\lambda_{F,e}$ is the positive root of the quadratic equation obtained by equating Eq. (35) to $F_{Th}$. In agreement with previous works [58,67], the threshold value is set to $F_{Th} = 0.5$. The function related to the failure load requirement is obtained by considering the inverse of the factor of safety:

$$f_F := \frac{pn\left(\lambda_{F,e}^{-1}\right) - \lambda_{F,Th}^{-1}}{\lambda_{F,Th}^{-1}} \approx \frac{\max_e\left(\lambda_{F,e}^{-1}\right) - \lambda_{F,Th}^{-1}}{\lambda_{F,Th}^{-1}} = \frac{\lambda_F^{-1} - \lambda_{F,Th}^{-1}}{\lambda_{F,Th}^{-1}}, \tag{37}$$

where $\lambda_{F,Th}$ is a threshold factor of safety. In this work, it is set equal to $\lambda_{F,RSol}$, i.e., to the factor of safety of RSol withstanding the reference LC. By considering Eqs. (33)–(35) and the expression of the $p$-norm operator, Eq. (37) reads:

$$f_F := \lambda_{F,Th}\left[\sum_e\left(\frac{-L_e + \sqrt{L_e^2 + 4Q_eF_{Th}}}{2Q_e}\right)^{-p}\right]^{1/p} - 1. \tag{38}$$

Of course, a negative value of $f_F$ means that the considered structure has a higher failure load than RSol.

The formal expression of the gradient of $f_F$ has been derived in a previous work [58] and it is recalled here below for the sake of completeness:

$$\begin{cases} \dfrac{\partial f_F}{\partial\xi^{(i_1,i_2)}} = -\left(\lambda_{F,Th}\right)^p\left(f_F+1\right)^{1-p}\left(l_{i_1i_2} + \boldsymbol{\upsilon}_F^T\tilde{\boldsymbol{\psi}}_{Ref,i_1i_2}\right), \\ \mathbf{K}_{FF}^*\ \boldsymbol{\upsilon}_{F,F}^* = -\boldsymbol{\psi}_{F,F}^*, \end{cases} \tag{39}$$

where:

- $l_{i_1i_2}$ is defined as:

$$l_{i_1i_2} := \sum_{e\in LS_{i_1i_2}}\left\{\frac{\partial\xi_e}{\partial\xi^{(i_1,i_2)}}\frac{\boldsymbol{\epsilon}_{Ref,e}^T}{\lambda_{F,e}^{p+1}Q_e\sqrt{\Delta_e}}\left[\left(F_{Th} - \lambda_{F,e}\sqrt{\Delta_e}\right)\frac{\partial}{\partial\xi_e}\left(\frac{\mathbf{G}_{Lam,e}}{t_e}\right)\boldsymbol{\epsilon}_{Ref,e} - \lambda_{F,e}Q_e\frac{\partial}{\partial\xi_e}\left(\frac{\mathbf{g}_{Lam,e}}{t_e}\right)\right]\right\}, \tag{40}$$

with $\Delta_e := L_e^2 + 4Q_eF_{Th}$.

- $\boldsymbol{\upsilon}_F^T := \left\{\boldsymbol{\upsilon}_{F,F}^{*\,T},\ \boldsymbol{\upsilon}_{F,D}^{*\,T}\right\}$ with $\boldsymbol{\upsilon}_{F,D}^* = \mathbf{0}$ is the auxiliary vector.
- $\boldsymbol{\psi}_F$ is defined as:

$$\boldsymbol{\psi}_F := \sum_e\left\{\frac{\mathfrak{L}_e^T\mathfrak{B}_e^T}{\lambda_{F,e}^{p+1}Q_e\sqrt{\Delta_e}}\left[2\left(F_{Th} - \lambda_{F,e}\sqrt{\Delta_e}\right)\frac{\mathbf{G}_{Lam,e}}{t_e}\boldsymbol{\epsilon}_{Ref,e}\ -\lambda_{F,e}Q_e\frac{\mathbf{g}_{Lam,e}}{t_e}\right]\right\}. \tag{41}$$

- $\tilde{\boldsymbol{\psi}}_{Ref,i_1i_2}$ is a fictitious force vector defined as:

$$\tilde{\boldsymbol{\psi}}_{Ref,i_1i_2} := \sum_{e\in LS_{i_1i_2}}\left(\frac{\partial\xi_e}{\partial\xi^{(i_1,i_2)}}\cdot\int_{A_e}\mathfrak{L}_e^T\mathfrak{B}_e^T\frac{\partial\mathbf{K}_{Lam,e}}{\partial\xi_e}\mathfrak{B}_e\mathfrak{L}_e dS\right)\mathbf{u}_{Ref}.$$

(42)

The analytical expression of the strength matrix $\mathbf{G}_{\text{Lam}}$ and vector $\mathbf{g}_{\text{Lam}}$ of the VSCL at the macroscopic scale and their gradient is available in [58].

In the considered design case, the reference LC for the evaluation of the response function $f_{\text{F}}$ is LC2.

### 3.2.4. Maximum tow curvature requirement

The design requirement on the maximum tow curvature has been formulated as an equivalent constraint in the PPs space only for the VSCLs belonging to sub-class C1 introduced in Section 2 [54,58]. These VSCLs are described by uniform values of $t$, $R_{0K}^{A^*}$ and $R_1^{A^*}$ (and, consequently, of $\tau$, $\alpha_0$ and $\alpha_1$), and a variable distribution of $\Phi_1^{A^*}$ (hence, of $\phi_1$) in the PPs framework. In the context of the FLP of the MS2LOS for VSCLs, a *laminate-level* conservative evaluation of the local curvature $\chi$ of the fibres, whose path in each $k$th layer is still unknown, is given by Izzi et al. [58]:

$$\chi(x,y) := \|\nabla\Phi_1(x,y)\| = \sqrt{\left(\frac{\partial\Phi_1}{\partial x}\right)^2 + \left(\frac{\partial\Phi_1}{\partial y}\right)^2} \geq \chi_k(x,y), \quad \forall\, k. \tag{43}$$

By denoting with $\chi_{\text{Th}}$ the maximum admissible curvature related to the manufacturing process, the manufacturability condition reads

$$\max_{x,y} \chi(x,y) \leq \chi_{\text{Th}}. \tag{44}$$

Regarding function $f_{\text{C}}$, the square of $\chi$ is used and the maximum operator is approximated via the $p$-Norm operator defined in Eq. (14), resulting in:

$$f_{\text{C}} := \frac{\left(\sum_e \left(\chi_e^2\right)^p\right)^{1/p} - \chi_{\text{Th}}^2}{\chi_{\text{Th}}^2} \approx \frac{\max_e \chi_e^2 - \chi_{\text{Th}}^2}{\chi_{\text{Th}}^2}, \tag{45}$$

where $\chi_e$ is the tow curvature computed at the centroid of the element $e$. As discussed by Izzi et al. [58], $\chi_e$ can be expressed in terms of the field $\phi_1$ as

$$\begin{aligned}\chi_e^2 &= \left(\frac{\pi}{2}\right)^2 \nabla\phi_1\big|_e^{\text{T}}\, \nabla\phi_1\big|_e \\ &= \left(\frac{\pi}{2}\right)^2 \left[\left(\frac{\partial\phi_1}{\partial u_1}\bigg|_e \cdot \frac{\partial u_1}{\partial x}\bigg|_e + \frac{\partial\phi_1}{\partial u_2}\bigg|_e \cdot \frac{\partial u_2}{\partial x}\bigg|_e\right)^2 \right. \\ &\quad \left. + \left(\frac{\partial\phi_1}{\partial u_1}\bigg|_e \cdot \frac{\partial u_1}{\partial y}\bigg|_e + \frac{\partial\phi_1}{\partial u_2}\bigg|_e \cdot \frac{\partial u_2}{\partial y}\bigg|_e\right)^2\right].\end{aligned} \tag{46}$$

In agreement with Eq. (7), the terms $(\partial\phi_1/\partial u_j)_e$ of Eq. (46) are of the type:

$$\frac{\partial^g}{\partial u_j}\bigg|_e = \sum_{i_1=0}^{n_1}\sum_{i_2=0}^{n_2}\left[\left(\frac{\mathrm{d}\left(N_{i_j,p_j}(u_j)\right)}{\mathrm{d}u_j}\bigg|_e N_{i_k,p_k}(u_{k\,e})\right)\xi^{(i_1,i_2)}\right] \tag{47}$$

for $j,k = 1,2$ with $j \neq k$.

According to Eq. (8), the partial derivative of the parametric coordinates $(u_1,u_2)$ with respect to the global ones $(x,y)$ reads

$$\begin{aligned}&\partial u_1/\partial x \equiv \partial u_2/\partial y = 1/l \\ &\partial u_1/\partial y \equiv \partial u_2/\partial x = 0.\end{aligned} \tag{48}$$

$f_{\text{C}}$ is, thus, a quadratic function of the design variables. The formal expression of the gradient of $f_{\text{C}}$ reads [58]:

$$\frac{\partial f_{\text{C}}}{\partial\xi^{(i_1,i_2)}} = \frac{\left(f_{\text{C}}+1\right)^{1-p}}{\left(\chi_{\text{Th}}^2\right)^p} \sum_{e\in LS_{i_1 i_2}} \left[\left(\chi_e^2\right)^{p-1} \frac{\partial\chi_e^2}{\partial\xi^{(i_1,i_2)}}\right], \tag{49}$$

**Table 5**
Threshold values used for the mathematical definition of the optimisation problem.

| Property | Unit | Value |
|---|---|---|
| $M_{\text{Th}} = M_{\text{DR,RSol}}$ | g | 935 |
| $\lambda_{\text{B,Th}} = \lambda_{\text{B,RSol}}$ | – | 1 |
| $\lambda_{\text{F,Th}} = \lambda_{\text{F,RSol}}$ | – | 1.37 |
| $\chi_{\text{Th}}$ | $\text{mm}^{-1}$ | 1/250 |

**Table 6**
Lower and upper bounds of the design variables.

| Design variable | Lower bound | Upper bound |
|---|---|---|
| $\tau^{(i_1,i_2)}$ | 0 | 2 |
| $\alpha_0^{(i_1,i_2)}$ | 0 | 1 |
| $\alpha_1^{(i_1,i_2)}$ | 0 | 1 |
| $\phi_1^{(i_1,i_2)}$ | −2 | +2 |

where

$$\frac{\partial\chi_e^2}{\partial\xi^{(i_1,i_2)}} = \begin{cases} \dfrac{\pi^2}{2}\, \nabla\phi_1\big|_e^{\text{T}} \cdot \dfrac{\partial\left(\nabla\phi_1\big|_e\right)}{\partial\phi_1^{(i_1,i_2)}} & \text{if } \xi = \phi_1, \\ 0 & \text{if } \xi \neq \phi_1. \end{cases} \tag{50}$$

### 3.3. Formulation of the optimisation problem

Considering the response functions representing the design requirements introduced in Section 2, the optimum design of the VSCL can be formulated as a CNLPP as follows:

$$\min_{\mathbf{x}} f_{\text{M}}(\mathbf{x}), \quad \text{s.t.} \begin{cases} f_{\text{B}}(\mathbf{x}) \leq 0, & \text{under LC1}, \\ f_{\text{F}}(\mathbf{x}) \leq 0, & \text{under LC2}, \\ f_{\text{C}}(\mathbf{x}) \leq 0, & (\text{only for VSCL} - \text{C1}). \end{cases} \tag{51}$$

The characteristics and mechanical performances of RSol have been used as threshold values for computing the response functions $f_{\text{M}}$, $f_{\text{B}}$ and $f_{\text{F}}$. For computing the response function $f_{\text{C}}$ and its gradient, the maximum admissible value of curvature proposed by Nagelsmith and Guerrits [68] as threshold value for $1/4''$ tows has been used. All these values are reported in Table 5. Finally, the value of the parameter $p$, involved in the definition of the $p$-Norm operator of Eq. (14), is set as $p = 848$ during the optimisation, computed through Eq. (15) for $d_{\max} = 0.01$ and $N_e^{\text{DR}} = 4608$ (see Section 4).

Problem (51) is solved for all sub-classes of VSCLs described in Section 2. A vector of design variables of different size is associated to each sub-class, as discussed in Section 3.1. The lower and upper bounds of the design variables are listed in Table 6.

## 4. Finite element model

The data needed to assess the structural responses introduced in Section 3.2 are recovered during the post-processing phase of linear static and eigenvalue buckling FE analyses performed in ANSYS APDL.

The FE model of the benchmark structure shown in Fig. 1 employed in these analyses is made of 4-node quadrilateral shell elements (ANSYS SHELL181) with six DOFs per node. The resulting mapped mesh is illustrated in Fig. 3. The overall number of elements composing the mesh has been set after a sensibility analysis (not reported here for the sake of brevity) whose goal is to find a good balance between computational costs and accuracy. The criterion of accuracy is related to both the approximation of the spatial distributions of the thickness and PPs over the structure, and to the evaluation of the mechanical responses of the structure. The whole model is composed of 9600 elements, while the DR of the structure is modelled through $N_e^{\text{DR}} = 4608$ elements.

Concerning the DR of the structure, the four independent fields describing the macroscopic behaviour of the VSCL, i.e., $\tau$, $\alpha_0$, $\alpha_1$, $\phi_1$,

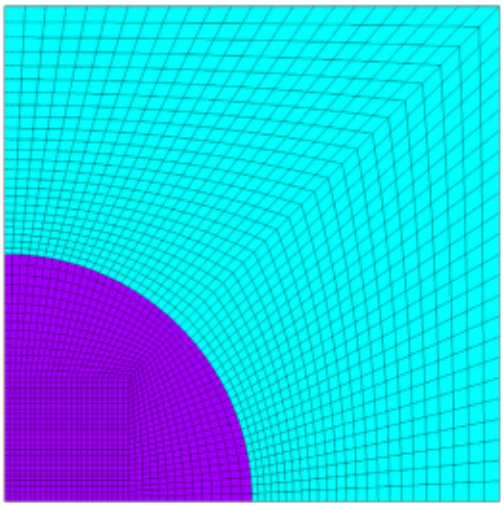

**Fig. 3.** Finite element model of the benchmark structure. Only the upper right quarter of it is shown.

**Table 7**
Parameters of the two employed optimisation algorithms (SLSQP and GCMMA) that have been set to a value different from their default one.

| Parameter SLSQP/GCMMA | Description | Value |
|---|---|---|
| `ftol/tol_f` | Tolerance on the relative difference between two consecutive function values at convergence | $10^{-5}$ |
| `/tol_p` | Minimum relative step between two consecutive points | $10^{-6}$ |
| `maxiter/max_it` | Maximum number of iterations | 300 |

are evaluated at the centroid of each element and the corresponding matrices $\mathbf{K}_{\mathrm{Lam},e}$, $\mathbf{G}_{\mathrm{Lam},e}$ and $\mathbf{g}_{\mathrm{Lam},e}$ [58] are assigned to such element. The properties of the elements modelling the porthole are kept constant during the optimisation and assigned in terms of thickness and elastic constants (reported in Tables 2 and 3, respectively).

The application of most of the BCs described in Fig. 1 and of the loads depicted in Fig. 2 is quite straightforward. The condition on the straightness of the outer edges of the structure is imposed through sets of constraint equations which couple the DOFs of the inner nodes of each edge to those of its vertices. All distributed loads are applied as equivalent resultant forces at the vertices of the edges.

## 5. Numerical results

The resolution of problem (51) has been carried through the numerical platform DOMES (Deterministic Optimisation of Macroscopic laminatEs via Splines) developed at the I2M laboratory in Bordeaux, where all design requirements presented in Section 3.2, together with their gradients, are implemented. DOMES is coded in Python language and represents an interface between the FE software and the optimisation algorithm, establishing a data structure for a modular implementation of the various requirements and for a simplified set-up of the design problem. With respect to the previous version [58], it has been updated with the implementation of the buckling requirement and the ability to deal with NDRs and multiple load cases.

Two optimisation algorithms are considered for the solution search: the Sequential Least-Squares Quadratic Programming (SLSQP) algorithm [69], included in the Python library SciPy v.1.4.1 [70], and the Globally Convergent Method of Moving Asymptotes (GCMMA) algorithm [71]. All parameters tuning the behaviour of the two algorithms have been set to their default values, except for those reported in Table 7.

**Table 8**
Sensitivity of the optimised solution to the number of control points when using the SLSQP algorithm or the GCMMA one.

| CPs | SLSQP | | | GCMMA | | |
|---|---|---|---|---|---|---|
| | $f_{\mathrm{M}}$ [%] | Stop crit. | Max constr. | $f_{\mathrm{M}}$ [%] | Stop crit. | Max constr. |
| $5 \times 5$ | −11.07 | max iter. | $2 \cdot 10^{-6}$ | −10.52 | conv. (iter. 277) | $< 0$ |
| $7 \times 7$ | −13.12 | max iter. | $2 \cdot 10^{-6}$ | −8.48 | max iter. | $10^{-6}$ |
| $9 \times 9$ | −13.82 | max iter. | $3 \cdot 10^{-4}$ | −12.62 | max iter. | $< 0$ |
| $11 \times 11$ | −14.57 | max iter. | $2 \cdot 10^{-4}$ | −8.71 | min step (iter. 96) | $< 0$ |
| $13 \times 13$ | −14.98 | max iter. | $3 \cdot 10^{-5}$ | −11.53 | max iter. | $< 0$ |
| $15 \times 15$ | −15.52 | max iter. | $1 \cdot 10^{-4}$ | −11.49 | max iter. | $< 0$ |
| $17 \times 17$ | −15.65 | max iter. | $1 \cdot 10^{-4}$ | −11.80 | max iter. | $< 0$ |
| $19 \times 19$ | −15.77 | max iter. | $2 \cdot 10^{-4}$ | −12.20 | max iter. | $< 0$ |
| $21 \times 21$ | −15.97 | max iter. | $4 \cdot 10^{-4}$ | −12.11 | max iter. | $< 0$ |

The reference solution RSol is characterised by the following values of the design variables: $\tau = 1$, $\alpha_0 = 0.5$, $\alpha_1 = 0$ (corresponding to $\rho_{0\mathrm{K}} = \rho_1 = 0$) and $\phi_1 = 0$. Moreover, RSol has been used as starting point for obtaining all results presented in this section.

As far as the integer parameters of the B-spline entities are concerned, the degrees of the Bernstein's polynomials have been set to $p_1 = p_2 = 2$, while the number of CPs is the outcome of a sensitivity analysis, which has also been used to compare the aforementioned optimisation algorithms. In this analysis, problem (51) has been solved in the design domain of VSCLs-C2 considering square CPs grids of various size with both algorithms. The results of this study are reported in Table 8 wherein, for each number of CPs, the value of the maximum constraint function and the type of stopping criterion satisfied at the end of the optimisation process is reported for both SLSQP and GCMMA algorithms. One can notice that, for this design application, the SLSQP algorithm provides optimised solutions characterised by a value of the cost function lower than that of the counterparts resulting from the GCMMA algorithm, for all considered CPs grids, although they are barely infeasible (the constraint violation is, in any case, very low and negligible from an engineering perspective). This is most likely due to GCMMA taking smaller and smaller steps and becoming trapped in a local minimum, as this algorithm (unlike the SLSQP algorithm) enforces the feasibility of the potential solution at each iteration. This feature is visualised in Fig. 4, wherein the iteration history of the cost and constraint functions for the optimisation process performed with the GCMMA algorithm for a $17 \times 17$ CPs grid is plotted. The analogous plot for the SLSQP algorithm is shown in Fig. 5. From the latter figure, it is clear that the SLSQP algorithm accepts violations of the constraints as long as significant reductions in the cost function can be obtained, and then reduces them in later iterations of the optimisation process as it approaches convergence.

A second observation that can be done looking at the results reported in Table 8 is that the sensitivity of the optimised solutions provided by the SLSQP algorithm to the number of CPs of the B-spline entity has a consistent behaviour: the higher the number of CPs the lower the final value of the cost function. This is not the case for the optimised solutions provided by the GCMMA algorithm. It has therefore been chosen to use the SLSQP algorithm with a $17 \times 17$ CPs grid, which corresponds to a total of 276 active CPs, i.e., CPs having elements of the DR in their local support. A comparison between the results provided by the algorithms SLSQP and GCMMA is provided in Appendix B.

In the following of this section, the results obtained for all considered VSCLs sub-classes are presented and commented. The optimised solutions are presented both in terms of their performances and of the optimised distributions of the PPs and of thickness over the structure. Regarding the latter, for improved readability, the distribution of the dimensionless PPs $\rho_{0K}$ and $\rho_1$ are provided instead of those of variables $\alpha_0$ and $\alpha_1$. The results are summarised in Table 9 wherein they are compared to RSol. In the case of a uniform field, the optimised value of the related variable is reported directly in such table, otherwise a figure (whose reference is reported in the table) is listed to show the

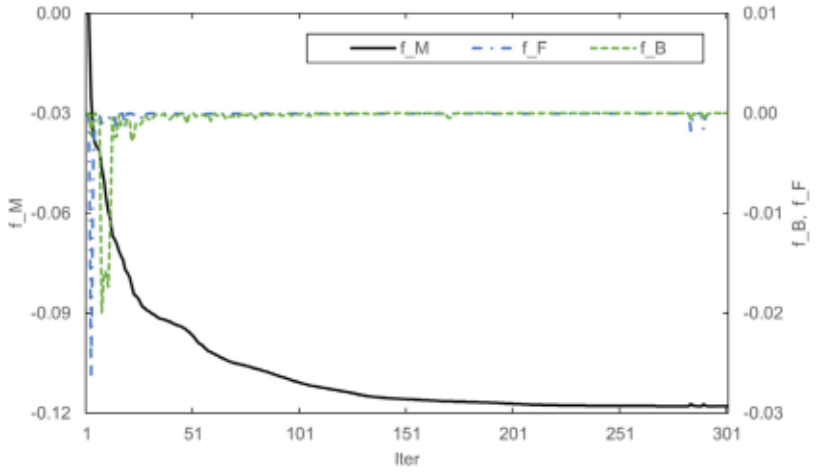


**Fig. 4.** Iteration history of the cost and constraint functions for the optimisation process of a VSCL-C2 (variable-stiffness composite laminate with uniform thickness and fully variable orthotropy) performed with the GCMMA algorithm.

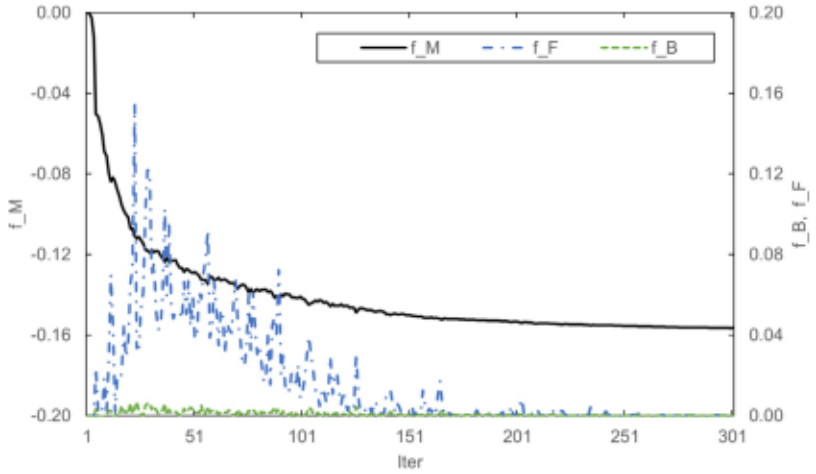


**Fig. 5.** Iteration history of the cost and constraint functions for the optimisation process of a VSCL-C2 (variable-stiffness composite laminate with uniform thickness and fully variable orthotropy) performed with the SLSQP algorithm.

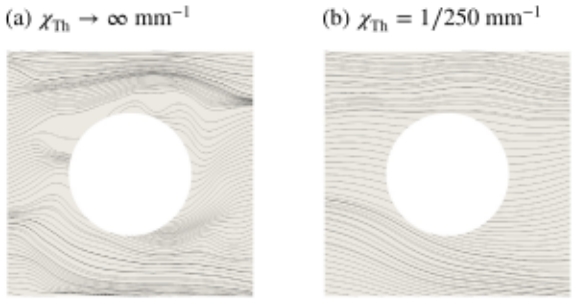


**Fig. 6.** Optimised VSCLs-C1 (variable-stiffness composite laminates with uniform thickness and variable orthotropy direction): streamlines of the optimal distribution of $\Phi_1^{A^*}$ obtained without (a) and with (b) the imposition of the constraint on the maximum tow curvature in Eq. (45).

optimised distribution of each non-uniform field. Moreover, in all the figures, the optimal field related to the main orthotropic direction $\Phi_1^{A*}$ is represented through streamlines plots.

From the results listed in Table 9, it can be noticed that optimised solutions show mass savings ranging from −5.6% to −19.8% with respect to RSol. Lighter solutions are obtained, as expected, when considering a less restrictive optimisation problem, either by removing the constraint on the tow curvature on VSCLs-C1 or by enlarging the design space, i.e., moving from VSCLs-C1 to VSCLs-C2 and VSCLs-C3. All the optimised solutions have performances practically identical to those of RSol, however they all are barely infeasible, with a maximum violated constraint of $4 \cdot 10^{-2}$.

**Table 9**
Summary of the optimised solutions.

| Solution | $f_M$ [%] | Max constr. | $\tau$ | $\rho_{0K}$ | $\rho_1$ | $\phi_1$ |
|---|---|---|---|---|---|---|
| RSol | 0 | 0 | 1 | 0.00 | 0.00 | 0.00 |
| C1 ($\chi_{Th}$ = 1/250 mm$^{-1}$) | −5.6 | $5 \cdot 10^{-3}$ | 0.944 | 0.00 | 0.03 | Fig. 6(a) |
| C1 ($\chi_{Th} \to \infty$ mm$^{-1}$)[a] | −10.3 | $6 \cdot 10^{-4}$ | 0.897 | 0.07 | 0.00 | Fig. 6(b) |
| C2 | −15.7 | $1 \cdot 10^{-4}$ | 0.844 | Fig. 8(a) | Fig. 8(b) | Fig. 8(c) |
| C3 | −19.8 | $4 \cdot 10^{-2}$ | Fig. 9(a) | Fig. 9(b) | Fig. 9(c) | Fig. 9(d) |
| C3 ($\lambda_{F,Th} = 1$) | −24.0 | $1 \cdot 10^{-2}$ | Fig. 11(a) | Fig. 11(b) | Fig. 11(c) | Fig. 11(d) |

[a] No constraint on the maximum tow curvature.

The last row of Table 9 shows the optimal VSCL-C3 obtained by solving a modified version of problem (51) wherein the threshold factor of safety of Eq. (37) has been set to $\lambda_{F,Th} = 1$. In this way, the least-weight, no-failure and no-buckling VSCL-C3 solution is obtained, which is about 24% lighter than RSol.

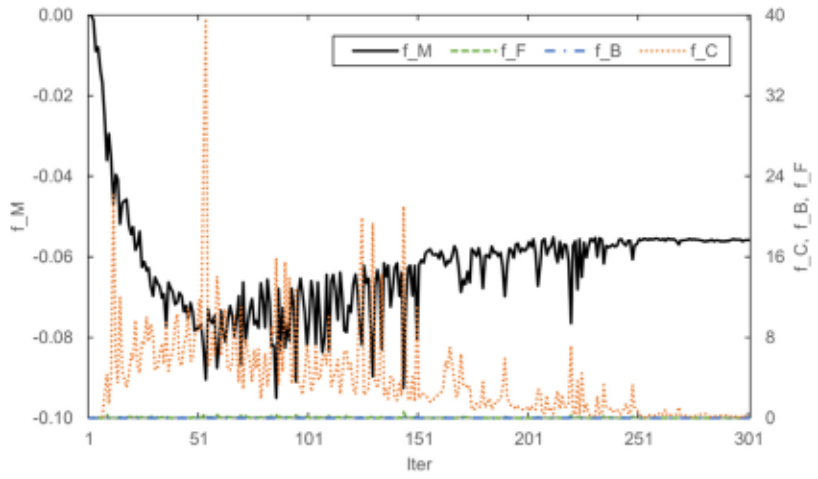


**Fig. 7.** Iteration history of the cost and constraint functions for the optimisation process leading to the VSCL-C1 solution (variable-stiffness composite laminate with uniform thickness and directionally variable orthotropy) subject to the maximum tow curvature constraint.

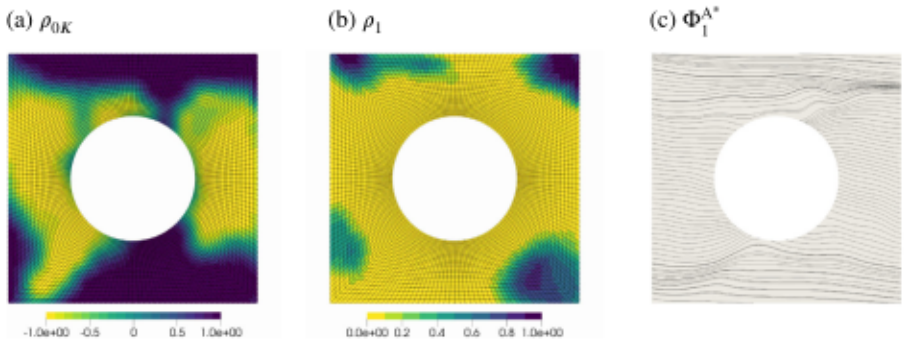


**Fig. 8.** Optimised VSCL-C2 (variable-stiffness composite laminate with uniform thickness and fully variable orthotropy): optimal distributions of the mechanical design variables.

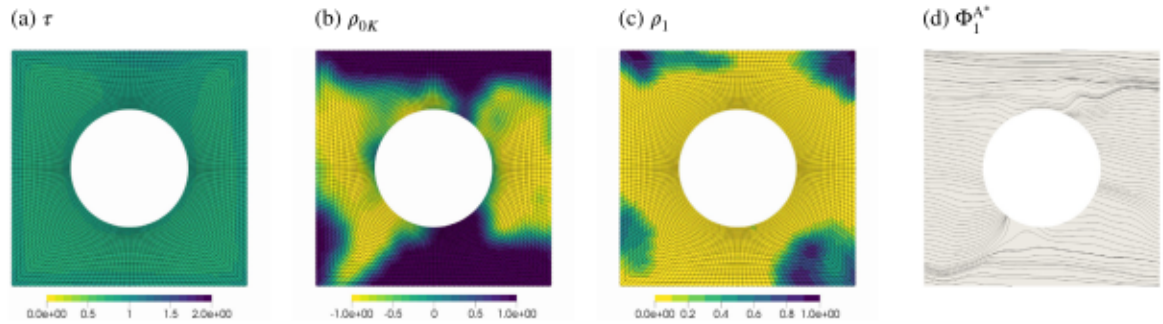


**Fig. 9.** Optimised VSCL-C3 (variable-stiffness composite laminate with variable thickness and fully variable orthotropy) obtained with $\lambda_{F,Th} = \lambda_{F,RSol}$: optimal distributions of the design variables.

From Table 9 one can notice that the optimised solution obtained for the sub-class C1 by imposing the constraint on the maximum tow curvature is characterised by an $R_0$-orthotropic behaviour [72], while the one obtained without imposing the curvature constraint presents a square orthotropy ($\rho_1 = 0$). In both cases optimal values of $\rho_{0K}$ and $\rho_1$ are very small, hence the mechanical behaviour is only slightly directional. However, this slight directionality has been exploited through a local tailoring of the main orthotropy direction (illustrated in Fig. 6) which allows these solutions to ensure the same performances of RSol with a weight-saving of 5.6% in presence of the curvature constraint, and of 10.3% when the constraint is not imposed. Fig. 6 allows also visualising the effect of the application of the constraint of the maximum tow curvature on obtained solutions in terms of the streamlines of the optimised distribution of $\Phi_1^{A^*}$. It is interesting to observe the iteration history of the cost and constraint functions for the optimisation process leading to the VSCL-C1 solution subject to the maximum tow curvature constraint, plotted in Fig. 7. As in all the other cases considered, the SLSQP algorithm is able to find a barely infeasible solution, although still technically acceptable. However, in this case it clearly has more difficulty in dealing with the maximum tow curvature constraint than with the other two involved: violations of the former are tens to hundreds of times higher throughout the iterations than those of the latter. This is probably due to the high value of the parameter $p$ used in the $p$-Norm operator, which makes the constraint function $f_C$ highly non-linear and could lead the algorithm to a new solution during iterations, characterised by a sudden change in the maximum tow curvature, explaining the spikes of the constraint function $f_C$ in Fig. 7.

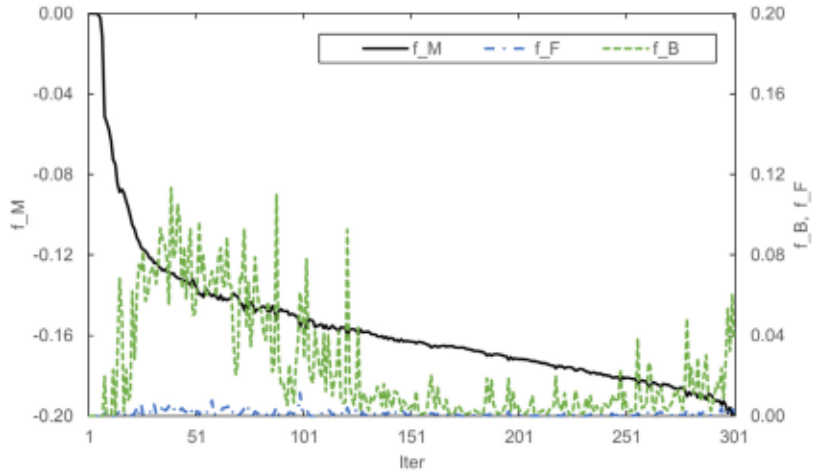


**Fig. 10.** Iteration history of the cost and constraint functions for the optimisation process leading to the VSCL-C3 solution (variable-stiffness composite laminate with variable thickness and fully variable orthotropy).

The possibility to locally optimise the orthotropy type as well as the main orthotropy direction is exploited in the case of the optimised solution obtained when considering the sub-class C2. This configuration allows to achieve a reduction of the mass of 15.7% with respect to RSol. When looking at the optimal distributions of the dimensionless PPs for this solution shown in Fig. 8, the following remarks can be drawn:

- $\rho_1 \to 0$ in a vast portion of the DR; this means that the local elastic behaviour is characterised by a square orthotropy ($\rho_{0K} \neq 0$) or isotropy ($\rho_{0K} = 0$).
- On the left and right sides of the porthole, $\rho_{0K}$ has a negative value (mainly close to $-1$), whilst $\rho_1 \to 0$, which corresponds to a square orthotropy with a high-shear-modulus behaviour.
- On the top and bottom regions of the porthole, $\rho_{0K}$ has a positive value (mainly close to 1), whilst $\rho_1 \to 0$, which corresponds to a square orthotropy with a low-shear-modulus behaviour.
- On the corner regions of the plate, both PPs have positive values and the VSCL has a classical orthotropic behaviour. More specifically, where $\rho_{0K} = \rho_1 = 1$ the VSCL behaves like a monolayer plate with the fibres locally oriented along the main axis of orthotropy.

By comparing Fig. 9 to Fig. 8, a strong similarity between the optimised solution obtained by considering the sub-class C3 (the most general one) and the optimised solution obtained for the sub-class C2 can be observed. The additional possibility of locally tailoring the thickness offered by VSCLs-C3 results in an optimal solution with a thickness distribution (Fig. 9(a)) characterised by thicker-than-average outer and inner (around the porthole) edges evolving towards a thinner intermediate region. This feature allows obtaining an optimised solution presenting a 19.8% mass reduction over RSol (an additional 4.1% with respect to its uniform-thickness counterpart, i.e., the optimised configuration obtained for sub-class C2).

Observing the iteration history of the optimisation process leading to the VSCL-C3 solution, plotted in Fig. 10, it is clear that convergence has not been achieved for this specific case. An even better solution could have been obtained by increasing the maximum number of iterations, which in this work was set at 300 (Table 7), a value considered acceptable for practical use.

Fig. 11 shows the optimal distribution of the design variables for the VSCL-C3 solution obtained with a value of $\lambda_{\mathrm{F,Th}} = 1$, i.e., by searching for a no-failure solution instead of a solution with a factor of safety higher than that of RSol. This solution presents many similarities with the optimised configuration shown in Fig. 9, but it is characterised by a more extended zone with a low-shear-modulus orthotropic behaviour (cf. Figs. 11(b) and 9(b)), and a thickness distribution evolving towards a thinner intermediate region (cf. Figs. 11(a) and 9(a)).

The distribution of $1/\lambda_{\mathrm{F},e}$ for RSol and all aforementioned optimal VSCL solutions is presented in Figs. 12 and 13. It can be clearly seen that, the higher the structural efficiency (moving from the optimised solution of sub-class C1 with constrained maximum tow curvature in Fig. 12(b) to the optimised solution of sub-class C3 in Fig. 13(a)), the more uniformly critical is the VSCL, with an increasing number of elements characterised by a value of $1/\lambda_{\mathrm{F},e} \to 1/\lambda_{\mathrm{F,RSol}}$. Of course, adopting a value of $\lambda_{\mathrm{F,Th}} = 1$ in problem (51) has an noticeable effect on the distribution of $1/\lambda_{\mathrm{F},e}$ for the related solution (Fig. 13(b)).

Finally, in Figs. 14 and 15, the buckling mode related to the first buckling load of the structure is presented for RSol and all optimal VSCL solutions. For Rsol and the optimised solutions of sub-classes C1 and C2 presented in Fig. 14, it is characterised by two opposed humps: a main slightly tilted and off-centre hump, and a smaller one located in the upper left corner of the structure (not always visible in the figure). However, the optimised solutions obtained for sub-class C3 present a different first buckling mode (Fig. 15): in addition to the two humps described above, a third one occurs, which interests the right hand side of the structure. It is most likely due to the presence in these solutions of a thicker zone around the porthole border (see Figs. 11(a) and 9(a)), which partially forces inflexion points in the structure.

## 6. Conclusions

A general theoretical/numerical methodology (with the related numerical tools) for the deterministic optimisation of variable-stiffness composite laminates (considering also general variable-thickness solutions) including design requirements on mass, buckling load, failure load, and manufacturability of the solution has been proposed in this work. The methodology deals with the first-level problem of the multi-scale two-level optimisation strategy for variable-stiffness composite laminates, hence it is focused exclusively on the macroscopic scale of the structure. On the one hand, the proposed approach relies on the polar method to describe the local macroscopic behaviour of the variable-stiffness composite laminate in terms of both elastic and strength properties (in the framework of the first-order shear deformation theory). On the other hand, the approach makes use of B-spline entities to represent the distribution of the design variables.

The approach presented in this work allows tailoring various properties of variable-stiffness composite laminates: the type of orthotropy and its direction, as well as the local thickness of the laminate. Various sub-classes of variable-stiffness composite laminates have been

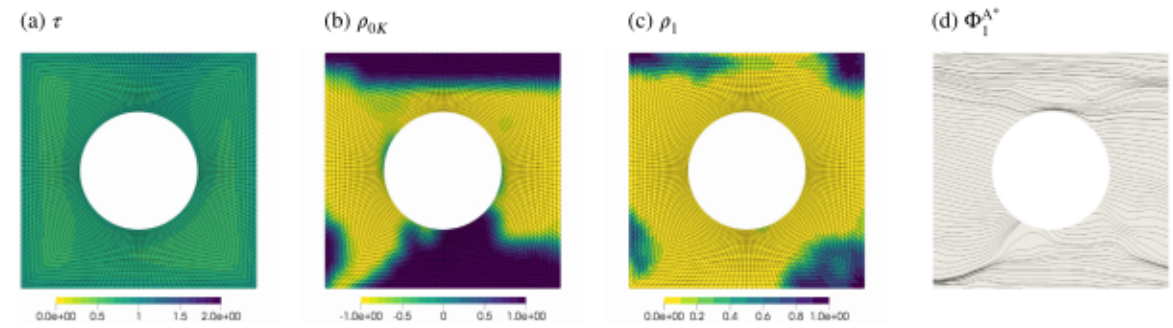


**Fig. 11.** Optimised VSCL-C3 (variable-stiffness composite laminate with variable thickness and fully variable orthotropy) obtained with $\lambda_{F,Th} = 1$: optimal distributions of the design variables.

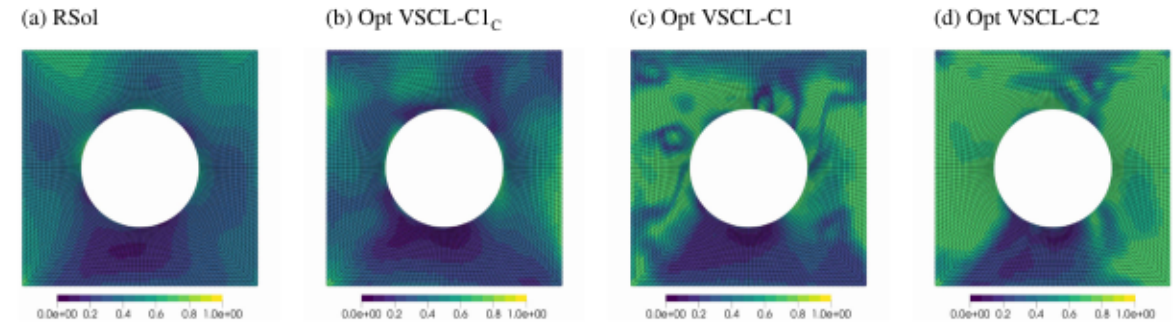


**Fig. 12.** Comparison of the distribution of $1/\lambda_{F,e}$ for RSol and some optimised solutions. Opt VSCL-C1$_C$ is the VSCL-C1 solution (variable-stiffness composite laminate with uniform thickness and variable orthotropy direction) found when the constraint on the maximum tow curvature is enforced ($\chi_{Th} = 1/250$ mm$^{-1}$).

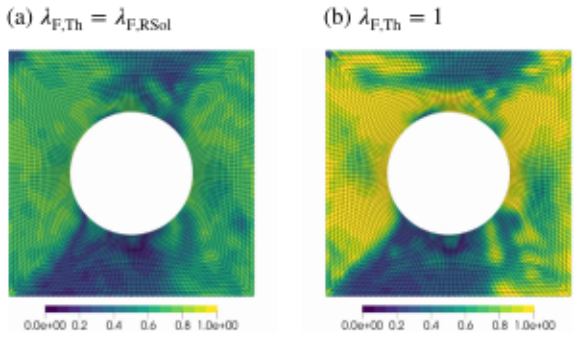


**Fig. 13.** Optimal VSCL*s*-C3 (variable-stiffness composite laminates with variable thickness and fully variable orthotropy): comparison of the distribution of $1/\lambda_{F,e}$ for the solutions obtained with $\lambda_{F,Th} = \lambda_{F,RSol}$ (a) and $\lambda_{F,Th} = 1$ (b).

introduced and investigated, by finding optimal solutions for each of them.

A meaningful design case is introduced and assessed in this work, i.e., the least-weight design of one of the panels composing a fuselage barrel having a plugged opening, withstanding pressurisation and other external loads. The structure is modelled through a square variable-stiffness composite plate with a central circular plastic porthole. The least-weight homogeneous isotropic version of the structure withstanding considered loads without buckling nor failure constitutes the reference solution and its mechanical performances are used as admissible values in the optimisation process. For the assessment of each requirement, an analytic response function and its gradient, formulated taking full advantage of the properties of the B-spline entities, are employed. The failure load of the structure is computed by applying a laminate-level failure criterion based on tensor invariants. The manufacturability of the solutions is checked both in terms of the point-wise condition on the existence of a suitable stack, and of a constraint on the maximum curvature of the filaments/tows composing the variable-stiffness composite laminate, formulated in the polar parameters space. For both these requirements and for the mass one, expressions of the functions previously derived by the authors have been employed. Conversely, regarding the buckling requirement, a new general expression of the response function and of its gradient has been derived here and implemented in the numerical platform DOMES.

Regarding numerical results, significant improvements with respect to the reference solution have been obtained through the proposed strategy. Optimal solutions show a mass reduction of the variable-stiffness composite laminate in the range 5.6%–19.8%, depending on the considered sub-class, while ensuring performances practically identical to those of the reference solution. For one of the considered variable-stiffness composite laminates sub-classes, not only the distribution of material elastic properties, but also the thickness distribution is optimised: the variable-thickness solution allows a 26% higher mass reduction than the best uniform-thickness solution. A second variable-thickness variable-stiffness solution is obtained simply enforcing the less restrictive yet more realistic no-buckling and no-failure requirements. This solution presents a 24% lighter variable-stiffness composite laminate than the reference solution.

The effectiveness of the proposed approach in dealing with realistic engineering problems involving multiple design requirements and complex load conditions is clearly shown through the obtained results. Moreover, these encouraging results highlight the great potential behind the various sub-classes of variable-stiffness composite laminates investigated in this work, motivating, thus, further research on this topic. Indeed, ongoing activities include: the formulation of new criteria to predict the presence of manufacturing-related defects, like filaments/tows gaps and/or overlaps, in the final structure, and to account for their effect on the performances since the preliminary design phase; the further generalisation of the design problem by concurrently optimising the in-plane topology, the polar parameters and the thickness of the laminate; the development of a more general formulation of the second-level problem (and of the related numerical

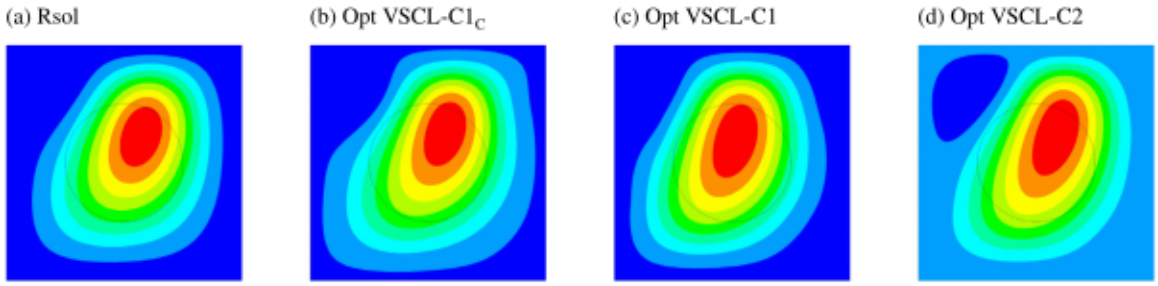


**Fig. 14.** Comparison of the first buckling mode (z component of the displacement) of RSol and of some optimised solutions. Opt VSCL-C1$_C$ is the VSCL-C1 solution (variable-stiffness composite laminate with uniform thickness and variable orthotropy direction) found when the constraint on the maximum tow curvature is enforced ($\chi_{Th} = 1/250$ mm$^{-1}$).

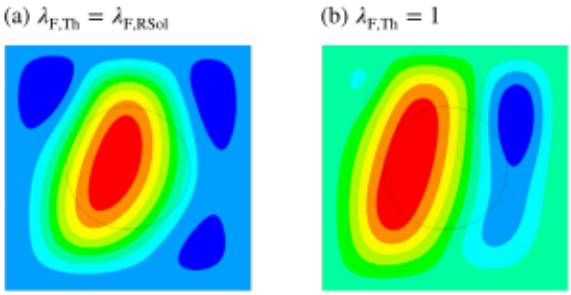


**Fig. 15.** Optimised VSCL*s*-C3 (variable-stiffness composite laminates with variable thickness and fully variable orthotropy): comparison of the first buckling mode (z component of the displacement) of the solutions obtained with $\lambda_{F,Th} = \lambda_{F,RSol}$ (a) and $\lambda_{F,Th} = 1$ (b).

tools) to recover the stack and the fibres-path within each lamina for all variable-stiffness composite laminates sub-classes; the application of the proposed strategy to variable-stiffness composite structures with single and double curvature.

## CRediT authorship contribution statement

**Michele Iacopo Izzi:** Conceptualization, Methodology, Investigation, Software, Validation, Data curation, Writing – original draft, Writing – review & editing, Visualization. **Marco Montemurro:** Conceptualization, Methodology, Software, Validation, Resources, Writing – original draft, Writing – review & editing, Supervision, Project administration, Funding acquisition. **Anita Catapano:** Conceptualization, Validation, Resources, Writing – review & editing, Supervision, Project administration, Funding acquisition.

## Declaration of competing interest

The authors declare that they have no known competing financial interests or personal relationships that could have appeared to influence the work reported in this paper.

## Data availability

Data will be made available on request.

## Acknowledgements

M. I. Izzi is grateful to Institut Carnot Arts for funding this work through the FA-COMP project. A. Catapano is grateful to French National Research Agency for funding this study through the research project COFFA (Conception et Optimisation de Forme pour la Fabrication Additive) ANR-17-CE10-0008. M. Montemurro is grateful to French National Research Agency for supporting this work through the research project GLAMOUR-VSC (Global-LocAl two-level Multi-scale optimisation strategy accOUnting for pRocess-induced singularities to design Variable Stiffness Composites) ANR-21-CE10-0014.

## Appendix A. Gradient of the buckling response function

Consider the energetic form of the classic eigenvalue buckling problem in the FE framework (specialised for the eigenvalue $\lambda_B$):

$$\mathbf{u}_B^T \left( \mathbf{K} + \lambda_B \mathbf{S}_{Ref} \right) \mathbf{u}_B = \mathbf{0}. \tag{A.1}$$

By differentiating Eq. (A.1), one can find the following expression of the derivative of $\lambda_B$ with respect to the design variable $\xi^{(i_1,i_2)}$:

$$\frac{\partial \lambda_B}{\partial \xi^{(i_1,i_2)}} = \frac{\lambda_B}{\mathbf{u}_B^T \mathbf{K} \mathbf{u}_B} \left( \mathbf{u}_B^T \frac{\partial \mathbf{K}}{\partial \xi^{(i_1,i_2)}} \mathbf{u}_B + \lambda_B \mathbf{u}_B^T \frac{\partial \mathbf{S}_{Ref}}{\partial \xi^{(i_1,i_2)}} \mathbf{u}_B \right). \tag{A.2}$$

The term $\mathbf{u}_B^T \mathbf{K} \mathbf{u}_B$ is the double of the strain energy $U_B$ associated to the buckling mode deformation.

Consider now the term $\frac{\partial \mathbf{K}}{\partial \xi^{(i_1,i_2)}} \mathbf{u}_B$ in Eq. (A.2). The stiffness matrix of the structure is defined as

$$\mathbf{K} := \sum_e \mathfrak{L}_e^T \mathbf{K}_e \mathfrak{L}_e. \tag{A.3}$$

$\mathbf{K}_e$ is the stiffness matrix of the element and, for a shell element, it is defined as

$$\mathbf{K}_e := \int_{A_e} \mathfrak{B}_e^T \mathbf{K}_{Lam,e} \mathfrak{B}_e dA, \tag{A.4}$$

where $A_e$ is the area of $e$th element. By taking into account for Eqs. (A.3) and (A.4) and for the local support property, the term $\frac{\partial \mathbf{K}}{\partial \xi^{(i_1,i_2)}} \mathbf{u}_B$ in Eq. (A.20) can be expressed as

$$\begin{aligned} \bar{\Psi}_{B,i_1 i_2} &:= \frac{\partial \mathbf{K}}{\partial \xi^{(i_1,i_2)}} \mathbf{u}_B \\ &= \sum_{e \in LS_{i_1 i_2}} \left[ \frac{\partial \xi_e}{\partial \xi^{(i_1,i_2)}} \int_{A_e} \mathfrak{L}_e^T \mathfrak{B}_e^T \frac{\partial \mathbf{K}_{Lam,e}}{\partial \xi_e} \mathfrak{B}_e \mathfrak{L}_e dA \right] \mathbf{u}_B, \end{aligned} \tag{A.5}$$

where the expression of the terms $\frac{\partial \mathbf{K}_{Lam,e}}{\partial \xi_e}$ can be found in [58].

Consider the quantity $\mathbf{u}_B^T \mathbf{S}_{Ref} \mathbf{u}_B$, which is the double of the non-linear (second-order) part of the internal work of the reference stress field over the additional strains due to the buckling mode $\mathbf{u}_B$:

$$\mathbf{u}_B^T \mathbf{S}_{Ref} \mathbf{u}_B := 2 W_{NL} \left( \sigma \left( \mathbf{u}_{Ref} \right), \varepsilon \left( \mathbf{u}_B \right) \right) = 2 \sum_e W_{NL,e} \left( \sigma \left( \mathbf{u}_{Ref} \right), \varepsilon \left( \mathbf{u}_B \right) \right), \tag{A.6}$$

$$\mathbf{R} = \begin{bmatrix} n_x & n_{xy} & \cdot & \cdot & \cdot & \cdot & \cdot & \cdot & m_x & m_{xy} & \cdot & \cdot & \cdot & q_x & \cdot \\ & n_y & \cdot & \cdot & \cdot & \cdot & \cdot & \cdot & m_{xy} & m_y & \cdot & \cdot & \cdot & q_y & \cdot \\ & & n_x & n_{xy} & \cdot & \cdot & -m_x & -m_{xy} & \cdot & \cdot & \cdot & \cdot & -q_x & \cdot & \cdot \\ & & & n_y & \cdot & \cdot & -m_{xy} & -m_y & \cdot & \cdot & \cdot & \cdot & -q_y & \cdot & \cdot \\ & & & & n_x & n_{xy} & \cdot & \cdot & \cdot & \cdot & \cdot & \cdot & \cdot & \cdot & \cdot \\ & & & & & n_y & \cdot & \cdot & \cdot & \cdot & \cdot & \cdot & \cdot & \cdot & \cdot \\ sym & & & & & & [ & & & & \mathbf{0}_{9\times 9} & & & & ] \end{bmatrix}. \tag{A.9}$$

**Box I.**

where

$$W_{\mathrm{NL},e}\left(\mathbf{f}_{\mathrm{Ref}}, \mathbf{u}_{\mathrm{B}}\right) := \frac{1}{2}\int_{A_e} \boldsymbol{\delta}_{\mathrm{B},e}^{\mathrm{T}} \mathbf{R}_{\mathrm{Ref},e} \boldsymbol{\delta}_{\mathrm{B},e}\, dA, \tag{A.7}$$

where $\boldsymbol{\delta}$ is a vector collecting the plate middle plane displacements partial derivatives (up to the first order) and the rotations, defined as

$$\begin{aligned} \boldsymbol{\delta}^{\mathrm{T}} := \Bigg\{ & \frac{\partial u_0}{\partial x}, \frac{\partial u_0}{\partial y}, \frac{\partial v_0}{\partial x}, \frac{\partial v_0}{\partial y}, \frac{\partial w_0}{\partial x}, \frac{\partial w_0}{\partial y}, \frac{\partial \theta_{x,0}}{\partial x}, \frac{\partial \theta_{x,0}}{\partial y}, \\ & \frac{\partial \theta_{y,0}}{\partial x}, \frac{\partial \theta_{y,0}}{\partial y}, \frac{\partial \theta_{z,0}}{\partial x}, \frac{\partial \theta_{z,0}}{\partial y}, \theta_{x,0}, \theta_{y,0}, \theta_{z,0} \Bigg\}, \end{aligned} \tag{A.8}$$

and $\mathbf{R}$ is the matrix of the generalised forces per unit length i.e., the components of vector $\mathbf{r}$ of Eq. (2), defined as in Box I. $\mathbf{R}$ is a linear function of the components of vector $\mathbf{r}$ and can be rewritten as

$$\mathbf{R} = \sum_i (\mathbf{r})_i\, \mathbf{O}_i, \tag{A.10}$$

where $\mathbf{O}_i$ are properly defined $15 \times 15$ matrices. By introducing $\mathfrak{G}_e$, i.e., the matrix relating the vectors $\boldsymbol{\delta}_e$ and $\mathbf{u}_e$, which is defined as

$$\mathfrak{G}_e : \mathbf{u}_e \mapsto \boldsymbol{\delta}_e, \quad \boldsymbol{\delta}_e = \mathfrak{G}_e \mathbf{u}_e, \tag{A.11}$$

by using Eq. (A.10), and by comparing Eq. (A.6) and (A.7), one obtains that

$$\mathbf{S}_{\mathrm{Ref}} := \sum_e \mathfrak{L}_e^{\mathrm{T}} \int_{A_e} \mathfrak{G}_e^{\mathrm{T}} \sum_i \left( \left(\mathbf{r}_{\mathrm{Ref},e}\right)_i \mathbf{O}_i \right) \mathfrak{G}_e\, dA\, \mathfrak{L}_e, \tag{A.12}$$

which can be approximated by

$$\mathbf{S}_{\mathrm{Ref}} \approx \sum_e \mathfrak{L}_e^{\mathrm{T}} \sum_i \left(\mathbf{r}_{\mathrm{Ref},e}\right)_i \int_{A_e} \mathfrak{G}_e^{\mathrm{T}} \mathbf{O}_i \mathfrak{G}_e\, dA\ \mathfrak{L}_e. \tag{A.13}$$

The expression provided in Eq. (A.13) allows highlighting the geometrical nature of the stress stiffness matrix $\mathbf{S}$: all the terms of the right hand side of the equation, except $\mathbf{r}_{\mathrm{Ref},e}$, only depend on geometrical properties of the $e$th element. Finally one can write

$$\mathbf{u}_{\mathrm{B}}^{\mathrm{T}} \mathbf{S}_{\mathrm{Ref}} \mathbf{u}_{\mathrm{B}} = \sum_e \mathbf{s}_{\mathrm{B},e}^{\mathrm{T}} \mathbf{r}_{\mathrm{Ref},e}, \tag{A.14}$$

where $\mathbf{s}_{\mathrm{B},e}$ is an $8 \times 1$ vector, whose components have been defined in Eq. (28). By employing Eqs. (A.14), (1) and (30), and by taking into account for the local support property, one can derive

$$\begin{aligned} \mathbf{u}_{\mathrm{B}}^{\mathrm{T}} \frac{\partial \mathbf{S}_{\mathrm{Ref}}}{\partial \xi^{(i_1,i_2)}} \mathbf{u}_{\mathrm{B}} &= \sum_e \mathbf{s}_{\mathrm{B},e}^{\mathrm{T}} \frac{\partial \mathbf{r}_{\mathrm{Ref},e}}{\partial \xi^{(i_1,i_2)}} \\ &= \sum_{e \in LS_{i_1 i_2}} \frac{\partial \xi_e}{\partial \xi^{(i_1,i_2)}} \mathbf{s}_{\mathrm{B},e}^{\mathrm{T}} \frac{\partial \mathbf{K}_{\mathrm{Lam},e}}{\partial \xi_e} \boldsymbol{\varepsilon}_{\mathrm{Ref},e} + \boldsymbol{\psi}_{\mathrm{B}}^{\mathrm{T}} \frac{\partial \mathbf{u}_{\mathrm{Ref}}}{\partial \xi^{(i_1,i_2)}}, \end{aligned} \tag{A.15}$$

where $\boldsymbol{\psi}_{\mathrm{B}}$ is the vector defined in Eq. (29). Consider the first and second of Eq. (12), with $\lambda = 1$:

$$\begin{aligned} \mathbf{K}_{\mathrm{FF}}^{*} \mathbf{u}_{\mathrm{Ref,F}}^{*} + \mathbf{K}_{\mathrm{FD}}^{*} \mathbf{u}_{\mathrm{Ref,D}}^{*} &= \mathbf{f}_{\mathrm{Ref,F}}^{*}, \\ \mathbf{K}_{\mathrm{DF}}^{*} \mathbf{u}_{\mathrm{Ref,F}}^{*} + \mathbf{K}_{\mathrm{DD}}^{*} \mathbf{u}_{\mathrm{Ref,D}}^{*} &= \mathbf{f}_{\mathrm{Ref,D}}^{*}. \end{aligned} \tag{A.16}$$

Inasmuch as external forces and known DOFs do not depend upon the design variables of the problem at hand, i.e.,

$$\frac{\partial \mathbf{f}_{\mathrm{Ref,F}}^{*}}{\partial \xi^{(i_1,i_2)}} = \mathbf{0}, \quad \frac{\partial \mathbf{u}_{\mathrm{Ref,D}}^{*}}{\partial \xi^{(i_1,i_2)}} = \mathbf{0}, \tag{A.17}$$

the derivative of Eq. (A.16) read

$$\begin{aligned} \mathbf{K}_{\mathrm{FF}}^{*} \frac{\partial \mathbf{u}_{\mathrm{Ref,F}}^{*}}{\partial \xi^{(i_1,i_2)}} + \frac{\partial \mathbf{K}_{\mathrm{FF}}^{*}}{\partial \xi^{(i_1,i_2)}} \mathbf{u}_{\mathrm{Ref,F}}^{*} + \frac{\partial \mathbf{K}_{\mathrm{FD}}^{*}}{\partial \xi^{(i_1,i_2)}} \mathbf{u}_{\mathrm{Ref,D}}^{*} &= \mathbf{0}, \\ \mathbf{K}_{\mathrm{DF}}^{*} \frac{\partial \mathbf{u}_{\mathrm{Ref,F}}^{*}}{\partial \xi^{(i_1,i_2)}} + \frac{\partial \mathbf{K}_{\mathrm{DF}}^{*}}{\partial \xi^{(i_1,i_2)}} \mathbf{u}_{\mathrm{Ref,F}}^{*} + \frac{\partial \mathbf{K}_{\mathrm{DD}}^{*}}{\partial \xi^{(i_1,i_2)}} \mathbf{u}_{\mathrm{Ref,D}}^{*} - \frac{\partial \mathbf{f}_{\mathrm{Ref,D}}^{*}}{\partial \xi^{(i_1,i_2)}} &= \mathbf{0}, \end{aligned} \tag{A.18}$$

Consider now the arbitrary auxiliary vector $\boldsymbol{\upsilon}_{\mathrm{B}}$, which can be reordered such that ${\boldsymbol{\upsilon}_{\mathrm{B}}^{*}}^{\mathrm{T}} := \left\{ {\boldsymbol{\upsilon}_{\mathrm{B,F}}^{*}}^{\mathrm{T}}, {\boldsymbol{\upsilon}_{\mathrm{B,D}}^{*}}^{\mathrm{T}} \right\}$. The following relation holds:

$$\begin{aligned} \boldsymbol{\psi}_{\mathrm{B}}^{\mathrm{T}} \frac{\partial \mathbf{u}_{\mathrm{Ref}}}{\partial \xi^{(i_1,i_2)}} = {\boldsymbol{\psi}_{\mathrm{B,F}}^{*}}^{\mathrm{T}} \frac{\partial \mathbf{u}_{\mathrm{Ref,F}}^{*}}{\partial \xi^{(i_1,i_2)}} + {\boldsymbol{\psi}_{\mathrm{B,D}}^{*}}^{\mathrm{T}} \underbrace{\frac{\partial \mathbf{u}_{\mathrm{Ref,D}}^{*}}{\partial \xi^{(i_1,i_2)}}}_{=\mathbf{0}} \\ + {\boldsymbol{\upsilon}_{\mathrm{B,F}}^{*}}^{\mathrm{T}} \underbrace{\left( \mathbf{K}_{\mathrm{FF}}^{*} \frac{\partial \mathbf{u}_{\mathrm{Ref,F}}^{*}}{\partial \xi^{(i_1,i_2)}} + \frac{\partial \mathbf{K}_{\mathrm{FF}}^{*}}{\partial \xi^{(i_1,i_2)}} \mathbf{u}_{\mathrm{Ref,F}}^{*} + \frac{\partial \mathbf{K}_{\mathrm{FD}}^{*}}{\partial \xi^{(i_1,i_2)}} \mathbf{u}_{\mathrm{Ref,D}}^{*} \right)}_{=\mathbf{0}} \\ + {\boldsymbol{\upsilon}_{\mathrm{B,D}}^{*}}^{\mathrm{T}} \underbrace{\left( \mathbf{K}_{\mathrm{DF}}^{*} \frac{\partial \mathbf{u}_{\mathrm{Ref,F}}^{*}}{\partial \xi^{(i_1,i_2)}} + \frac{\partial \mathbf{K}_{\mathrm{DF}}^{*}}{\partial \xi^{(i_1,i_2)}} \mathbf{u}_{\mathrm{Ref,F}}^{*} + \frac{\partial \mathbf{K}_{\mathrm{DD}}^{*}}{\partial \xi^{(i_1,i_2)}} \mathbf{u}_{\mathrm{Ref,D}}^{*} - \frac{\partial \mathbf{f}_{\mathrm{Ref,D}}^{*}}{\partial \xi^{(i_1,i_2)}} \right)}_{=\mathbf{0}}, \end{aligned} \tag{A.19}$$

Eq. (A.19) simplifies to

$$\begin{aligned} \boldsymbol{\psi}_{\mathrm{B}}^{\mathrm{T}} \frac{\partial \mathbf{u}_{\mathrm{Ref}}}{\partial \xi^{(i_1,i_2)}} \equiv & \left( {\boldsymbol{\psi}_{\mathrm{B,F}}^{*}}^{\mathrm{T}} + {\boldsymbol{\upsilon}_{\mathrm{B,F}}^{*}}^{\mathrm{T}} \mathbf{K}_{\mathrm{FF}}^{*} + {\boldsymbol{\upsilon}_{\mathrm{B,D}}^{*}}^{\mathrm{T}} \mathbf{K}_{\mathrm{DF}}^{*} \right) \frac{\partial \mathbf{u}_{\mathrm{Ref,F}}^{*}}{\partial \xi^{(i_1,i_2)}} \\ & - {\boldsymbol{\upsilon}_{\mathrm{B,D}}^{*}}^{\mathrm{T}} \frac{\partial \mathbf{f}_{\mathrm{Ref,D}}^{*}}{\partial \xi^{(i_1,i_2)}} + \boldsymbol{\upsilon}_{\mathrm{B}}^{\mathrm{T}} \frac{\partial \mathbf{K}}{\partial \xi^{(i_1,i_2)}} \mathbf{u}_{\mathrm{Ref}}. \end{aligned} \tag{A.20}$$

The above formula can be further simplified. Consider the term $\bar{\boldsymbol{\psi}}_{\mathrm{Ref},i_1 i_2}$ defined as

$$\bar{\boldsymbol{\psi}}_{\mathrm{Ref},i_1 i_2} := \frac{\partial \mathbf{K}}{\partial \xi^{(i_1,i_2)}} \mathbf{u}_{\mathrm{Ref}}. \tag{A.21}$$

By using Eqs. (A.3) and (A.4), and by taking into account for the local support property, Eq. (A.21) can be expressed as

$$\bar{\boldsymbol{\psi}}_{\mathrm{Ref},i_1 i_2} = \sum_{e \in LS_{i_1 i_2}} \left[ \frac{\partial \xi_e}{\partial \xi^{(i_1,i_2)}} \int_{A_e} \mathfrak{L}_e^{\mathrm{T}} \mathfrak{B}_e^{\mathrm{T}} \frac{\partial \mathbf{K}_{\mathrm{Lam},e}}{\partial \xi_e} \mathfrak{B}_e \mathfrak{L}_e dA \right] \mathbf{u}_{\mathrm{Ref}}. \tag{A.22}$$

Moreover, the components of the arbitrary vector $\boldsymbol{\upsilon}_{\mathrm{B}}$ can be chosen in such a way that the terms multiplying $\frac{\partial \mathbf{u}_{\mathrm{Ref,F}}}{\partial \xi^{(i_1,i_2)}}$ and $\frac{\partial \mathbf{f}_{\mathrm{Ref,D}}^{*}}{\partial \xi^{(i_1,i_2)}}$ vanish, i.e.,

$$\begin{cases} \mathbf{K}_{\mathrm{FF}}^{*} \boldsymbol{\upsilon}_{\mathrm{B,F}}^{*} = -\boldsymbol{\psi}_{\mathrm{B,F}}^{*}, \\ \boldsymbol{\upsilon}_{\mathrm{B,D}}^{*} = \mathbf{0}. \end{cases} \tag{A.23}$$

By using Eq. (A.21) and the expression of $\boldsymbol{\upsilon}_{\mathrm{B}}^{*}$ obtained by solving the auxiliary system of Eq. (A.23), Eq. (A.20) simplifies to

$$\boldsymbol{\psi}_{\mathrm{B}}^{\mathrm{T}} \frac{\partial \mathbf{u}_{\mathrm{Ref}}}{\partial \xi^{(i_1,i_2)}} = \boldsymbol{\upsilon}_{\mathrm{B}}^{\mathrm{T}} \bar{\boldsymbol{\psi}}_{\mathrm{Ref},i_1 i_2}. \tag{A.24}$$

Therefore, the final expression of the generic component of the gradient of $f_{\mathrm{B}}$ defined in Eq. (23) can be obtained through Eqs. (A.2), (A.5),

**Table B.1**
Comparison of optimised VSCLs-C2 (variable-stiffness composite laminate with uniform thickness fully variable orthotropy) obtained through the CGMMA algorithm and the SLSQP one.

| Solution | Starting point | $f_M$ [%] | Max constr. | $\tau$ | $\rho_{0K}$ | $\rho_1$ | $\Phi_1$ |
|---|---|---|---|---|---|---|---|
| RSol | – | 0 | 0 | 1 | 0.00 | 0.00 | 0.00 |
| C2-SLSQP | RSol | −15.65 | $1 \cdot 10^{-4}$ | 0.844 | Fig. 8(a) | Fig. 8(b) | Fig. 8(c) |
| C2-GCMMA | | −11.80 | $< 0$ | 0.882 | Fig. B.2(a) | Fig. B.2(b) | Fig. B.2(c) |
| Rnd | – | – | – | 1.932 | Fig. B.1(a) | Fig. B.1(b) | Fig. B.1(c) |
| $C2_{Rnd}$-SLSQP | Rnd | −13.74 | $1 \cdot 10^{-3}$ | 0.863 | Fig. B.3(a) | Fig. B.3(b) | Fig. B.3(c) |
| $C2_{Rnd}$-GCMMA | | −3.53 | $< 0$ | 0.965 | Fig. B.4(a) | Fig. B.4(b) | Fig. B.4(c) |

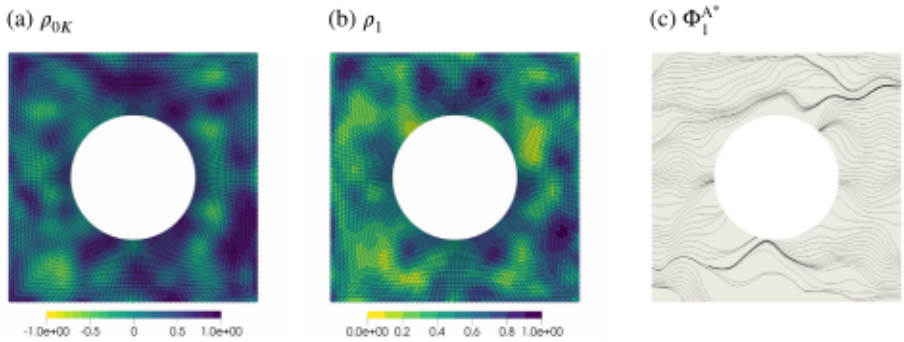


**Fig. B.1.** Random (Rnd) VSCL-C2 (variable-stiffness composite laminate with uniform thickness fully variable orthotropy) used as starting point for the comparison between the optimisation algorithms SLSQP and GCMMA.

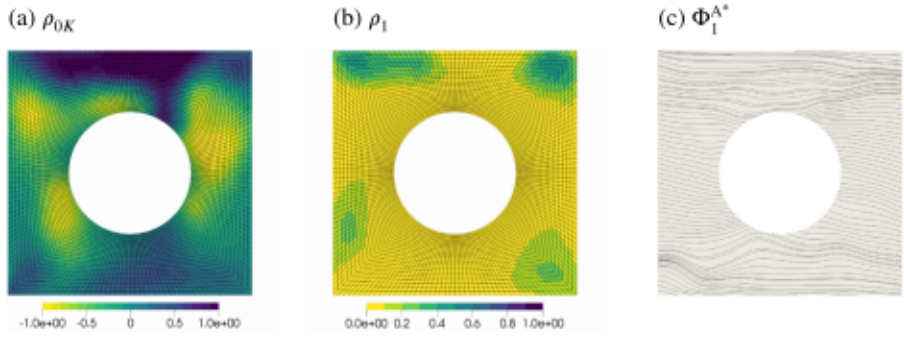


**Fig. B.2.** Distributions of the mechanical design variables for the optimised VSCL-C2 (variable-stiffness composite laminate with uniform thickness fully variable orthotropy) found by the CGMMA algorithm (solution C2-GCMMA).

(A.15) and (A.24):

$$\frac{\partial f_B}{\partial \xi^{(i_1,i_2)}} = -\frac{\lambda_B}{2U_B \lambda_{B,Th}} \left[ \mathbf{u}_B^T \bar{\Psi}_{B,i_1 i_2} + \lambda_B \left( \sum_{e \in LS_{i_1 i_2}} \frac{\partial \xi_e}{\partial \xi^{(i_1,i_2)}} \mathbf{s}_{B,e}^T \frac{\partial \mathbf{K}_{Lam,e}}{\partial \xi_e} \boldsymbol{\varepsilon}_{Ref,e} + \boldsymbol{v}_B^T \bar{\Psi}_{Ref,i_1 i_2} \right) \right]. \tag{A.25}$$

It is noteworthy that the solution of the auxiliary system of Eq. (A.23), needed to compute the gradient of $f_B$, can be obtained through a FE analysis wherein all DOFs corresponding to the known DOFs of Eq. (12) are set equal to zero, i.e., $\boldsymbol{v}_{B,D}^* = \mathbf{0}$, and whose generalised external nodal forces $\boldsymbol{\psi}_B$ are computed using Eq. (29). Of course, the components of $\boldsymbol{\psi}_B$ corresponding to the known DOFs of Eq. (12), i.e., $\boldsymbol{\psi}_{B,D}^*$, are discarded by the FE solver because applied on constrained DOFs.

## Appendix B. A comparison between results from SLSQP and GCMMA algorithms

In this section, two sets of solutions obtained using the SLSQP algorithm and the GCMMA one are presented for comparison purposes. The optimal results for these solution are collected in Table B.1, which is complemented by Figs. 8, B.2, B.3 and B.4. For the two sets, problem (51) has been solved with both algorithms in the design domain of VSCLs-C2 considering a control grid made of 17 × 17 CPs. The first set of results is obtained using RSol as starting point, while the same random distribution of design variables (named Rnd and represented in Fig. B.1) is used for obtaining the second set.

As far as the first set of results is concerned, clear similarities can be observed between the optimal distributions of the design variables obtained by GCMMA and SLSQP (cf. Figs. B.2 and 8). This is a strong hint that both algorithms followed similar paths during the solution search, however the final solution provided by GCMMA is characterised by a value of the cost function that is higher than the one of the SLSQP solution. This is most likely due to GCMMA adopting increasingly smaller steps and getting trapped into a local minimum because this algorithm enforces the feasibility of the potential solution at each iteration (unlike SLSQP algorithm).

The second set of results, obtained using Rnd as starting point, is shown in Figs. B.3 and B.4. The complete randomness of the starting distributions of the design variables in Rnd (Fig. B.1) leads to optimal distributions characterised by a higher degree of non-uniformity with

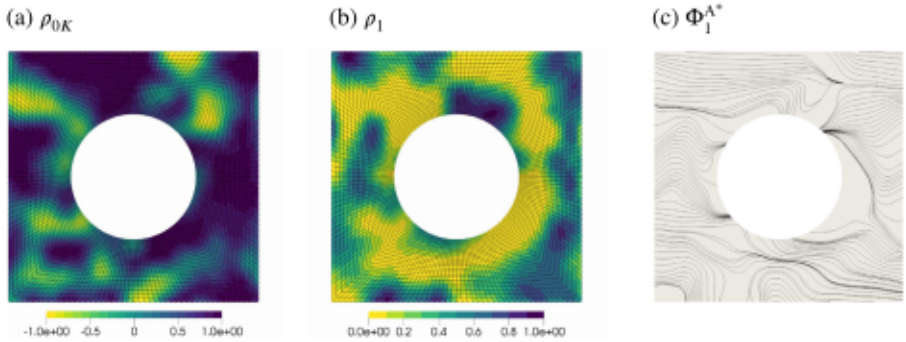


**Fig. B.3.** Distributions of the mechanical design variables for the optimal VSCL-C2 (variable-stiffness composite laminate with uniform thickness fully variable orthotropy) found by the SLSQP algorithm when using Rnd as starting point (solution $C2_{Rnd}$-SLSQP).

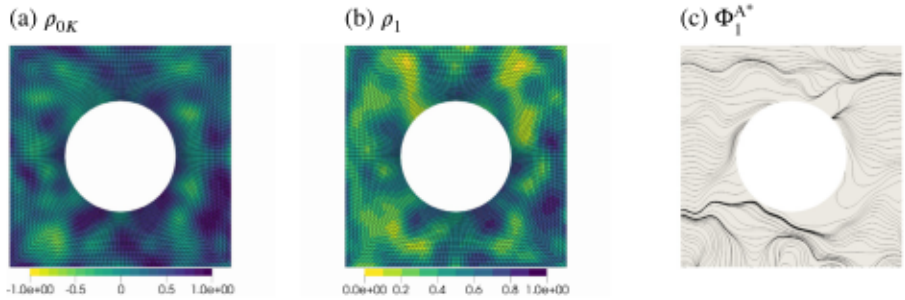


**Fig. B.4.** Distributions of the mechanical design variables for the optimal VSCL-C2 (variable-stiffness composite laminate with uniform thickness fully variable orthotropy) found by the GCMMA algorithm when using Rnd as starting point (solution $C2_{Rnd}$-GCMMA).

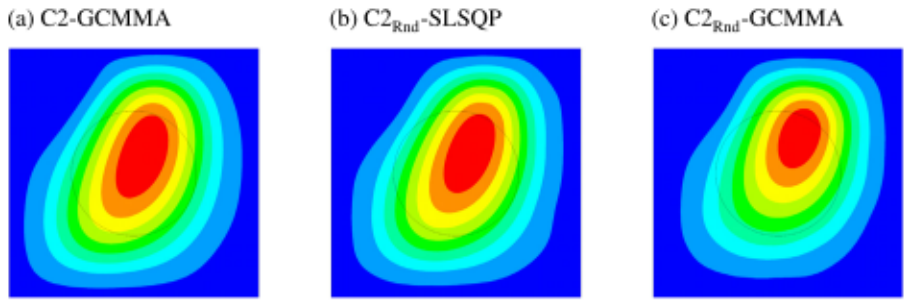


**Fig. B.5.** Comparison of the first buckling mode (z component of the displacement) of optimised VSCLs-C2 (variable-stiffness composite laminates with uniform thickness fully variable orthotropy) obtained through the CGMMA algorithm and the SLSQP one.

respect to the one of the solutions previously presented. However, SLSQP does a better job in smoothing the design variable fields which results into a better solution (in terms of the value of the objective function) than the one provided by GCMMA. Nevertheless, it is noteworthy that the solutions provided by the SLSQP algorithm are always barely infeasible (but still acceptable from an engineering standpoint) because the maximum value of the optimisation constraints is positive at the end of the optimisation process.

Finally, the buckling mode related to the first buckling load of the structure for the solutions listed in Table B.1 is shown in Fig. B.5 (the buckling mode for solution C2-SLSQP is shown in Fig. 14(d)). For all solutions, it has the same characteristics of the buckling modes in Fig. 14(d), i.e, it is a two-humps mode with a main slightly tilted and off-centre hump, and a smaller one located in the upper left corner of the structure (not visible in the figure).

## References

[1] Murugan V, Alaimo G, Auricchio F, Marconi S. An orientation-field based algorithm for free-form material extrusion. Addit Manuf 2022;59:103064.

[2] Karaş B, Smith PJ, Fairclough JPA, Mumtaz K. Additive manufacturing of high density carbon fibre reinforced polymer composites. Addit Manuf 2022;58:103044.

[3] Catapano A, Montemurro M, Balcou J-A, Panettieri E. Rapid prototyping of variable angle-tow composites. Aerotecnica Missili & Spazio 2019;98(4):257–71.

[4] Shiratori H, Todoroki A, Ueda M, Matsuzaki R, Hirano Y. Mechanism of folding a fiber bundle in the curved section of 3D printed carbon fiber reinforced plastics. Int J Mech Sci 2020;29(3):247–57.

[5] Akhavan H, Ribeiro P, de Moura M. Large deflection and stresses in variable stiffness composite laminates with curvilinear fibres. Int J Mech Sci 2013;73:14–26.

[6] Chen X, Nie G, Wu Z. Application of Rayleigh-Ritz formulation to thermomechanical buckling of variable angle tow composite plates with general in-plane boundary constraint. Int J Mech Sci 2020;187:106094.

[7] Alhajahmad A, Mittelstedt C. Buckling and postbuckling performance of composite fuselage panels with cutouts using continuous streamline fibres. Int J Mech Sci 2021;212:106841.

[8] Donough MJ, Shafaq, St John NA, Philips AW, Gangadhara Prusty B. Process modelling of In-situ consolidated thermoplastic composite by automated fibre placement – A review. Composites A 2022;163:107179.

[9] Wehbe R, Tatting B, Rajan S, Harik R, Sutton M, Gürdal Z. Geometrical modeling of tow wrinkles in automated fiber placement. Compos Struct 2020;246:112394.

[10] Kim BC, Potter K, Weaver PM. Continuous tow shearing for manufacturing variable angle tow composites. Composites A 2012;43(8):1347–56.

[11] Macquart T, Bordogna MT, Lancelot P, Breuker RD. Derivation and application of blending constraints in lamination parameter space for composite optimisation. Compos Struct 2016;135:224–35.

[12] Panettieri E, Montemurro M, Catapano A. Blending constraints for composite laminates in polar parameters space. Composites B 2019;168:448–57.

[13] Picchi Scardaoni M, Montemurro M, Panettieri E, Catapano A. New blending constraints and a stack-recovery strategy for the multi-scale design of composite laminates. Struct Multidiscip Optim 2021;63:741–66.

[14] Ghiasi H, Fayazbakhsh D, Pasini D, Lessard L. Optimum stacking sequence design of composite materials part II: Variable stiffness design. Compos Struct 2010;93:1–13.

[15] Albazzan M, Harik R, Tatting B, Gürdal Z. Efficient design optimization of nonconventional laminated composites using lamination parameters: A state of the art. Compos Struct 2019;209:362–74.

[16] Hyer M, Lee H. The use of curvilinear fiber format to improve buckling resistance of composite plates with central circular holes. Compos Struct 1991;18(3):239–61.

[17] Hyer M, Charette R. Use of curvilinear fiber format in composite structure design. AIAA J 1991;29(6):1011–5.

[18] Gurdal Z, Olmedo R. In-plane response of laminates with spatially varying fiber orientations - Variable stiffness concept. AIAA J 1993;31(4):751–8.

[19] Alhajahmad A, Abdalla M, Gürdal Z. Optimal design of a pressurized fuselage panel with a cutout using tow-placed steered fibers. In: Proceedings of the international conference on engineering optimization 2008. 2008.

[20] Huang J, Haftka R. Optimization of fiber orientations near a hole for increased load-carrying capacity of composite laminates. Struct Multidiscip Optim 2005;30(5):335–41.

[21] Nagendra S, Kodiyalam S, Davis J, Parthasarathy V. Optimization of tow fiber paths for composite design. In: 36th structures, structural dynamics and materials conference. American Institute of Aeronautics and Astronautics; 1995, http://dx.doi.org/10.2514/6.1995-1275.

[22] Tian Y, Pu S, Shi T, Xia Q. A parametric divergence-free vector field method for the optimization of composite structures with curvilinear fibers. Comput Methods Appl Mech Engrg 2021;373:113574.

[23] Cao Z, Lin G, Shi Q, Cao Q. Optimization analysis of NURBS curved variable stiffness laminates with a hole. Mater Today Commun 2022;31:103364.

[24] Ding H, Xu B, Li W, Huang X. A novel CS-RBFs-based parameterization scheme for the optimization design of curvilinear variable-stiffness composites with manufacturing constraints. Compos Struct 2022;299:116067.

[25] Alhajahmad A, Mittelstedt C. Buckling capacity of composite panels with cutouts using continuous curvilinear fibres and stiffeners based on streamlines. Compos Struct 2022;281:114974.

[26] Khan S, Fayazbakhsh K, Fawaz Z, Arian Nik M. Curvilinear variable stiffness 3D printing technology for improved open-hole tensile strength. Addit Manuf 2018;24:378–85.

[27] Nik MA, Fayazbakhsh K, Khan S, Fawaz Z. Strength evaluation of continuous curvilinear variable stiffness panels with circular cutouts under biaxial normal loading and off-design conditions. Mech Adv Mater Struct 2021;1–14.

[28] Shafighfard T, Cender TA, Demir E. Additive manufacturing of compliance optimized variable stiffness composites through short fiber alignment along curvilinear paths. Addit Manuf 2021;37:101728.

[29] Khan S, Nik MA, Fayazbakhsh K, Fawaz Z. Continuous curvilinear variable stiffness design for improved strength of a panel with a cutout. Mech Adv Mater Struct 2022;29(7):975–83.

[30] de Kergariou C, Kim BC, Perriman A, Le Duigou A, Guessasma S, Scarpa F. Design of 3D and 4D printed continuous fibre composites via an evolutionary algorithm and voxel-based finite elements: Application to natural fibre hygromorphs. Addit Manuf 2022;59:103144.

[31] Ghayoor H, Rouhi M, Hoa SV, Hojjati M. Use of curvilinear fibers for improved bending-induced buckling capacity of elliptical composite cylinders. Int J Solids Struct 2017;109:112–22.

[32] Rouhi M, Ghayoor H, Hoa SV, Hojjati M. Multi-objective design optimization of variable stiffness composite cylinders. Composites B 2015;69:249–55.

[33] Rouhi M, Ghayoor H, Hoa SV, Hojjati M. Effect of structural parameters on design of variable-stiffness composite cylinders made by fiber steering. Compos Struct 2014;118:472–81.

[34] Arian Nik M, Fayazbakhsh K, Pasini D, Lessard L. Optimization of variable stiffness composites with embedded defects induced by automated fiber placement. Compos Struct 2014;107:160–6.

[35] Arian Nik M, Fayazbakhsh K, Pasini D, Lessard L. Surrogate-based multi-objective optimization of a composite laminate with curvilinear fibers. Compos Struct 2012;94(8):2306–13.

[36] Passos A, Luersen M, Steeves C. Optimal curved fibre orientations of a composite panel with cutout for improved buckling load using the efficient global optimization algorithm. Eng Optim 2017;49(8):1354–72.

[37] Cao Z, Dong M, Shi Q, Han Z, Qiu R. Research on buckling characteristics and placement processability of variable stiffness open-hole laminates. Composites C 2022;7:100233.

[38] Coskun O, Turkmen HS. Multi-objective optimization of variable stiffness laminated plates modeled using Bézier curves. Compos Struct 2022;279:114814.

[39] Yoo K, Bacarreza O, Aliabadi M. A novel multi-fidelity modelling-based framework for reliability-based design optimisation of composite structures. Eng Comput 2020;38:595–608.

[40] Pan Z, Zhang L-W, Liew K. Adaptive surrogate-based harmony search algorithm for design optimization of variable stiffness composite materials. Comput Methods Appl Mech Engrg 2021;379:113754.

[41] Guo Q, Hang J, Wang S, Hui W, Xie Z. Design optimization of variable stiffness composites by using multi-fidelity surrogate models. Struct Multidiscip Optim 2021;63:439–61.

[42] Guo Q, Hang J, Wang S, Hui W, Xie Z. Buckling optimization of variable stiffness composite cylinders by using multi-fidelity surrogate models. Thin-Walled Struct 2020;156:107014.

[43] Rouhi M, Ghayoor H, Hoa SV, Hojjati M. Computational efficiency and accuracy of multi-step design optimization method for variable stiffness composite structures. Thin-Walled Struct 2017;113:136–43.

[44] Rouhi M, Ghayoor H, Hoa SV, Hojjati M, Weaver PM. Stiffness tailoring of elliptical composite cylinders for axial buckling performance. Compos Struct 2016;150:115–23.

[45] Passos A, Luersen M. Multiobjective optimization of laminated composite parts with curvilinear fibers using Kriging-based approaches. Struct Multidiscip Optim 2018;57:1115–27.

[46] Wu Z, Raju G, Weaver PM. Framework for the buckling optimization of variable-angle tow composite plates. AIAA J 2015;53(12):3788–804.

[47] Khani A, IJsselmuiden ST, Abdalla MM, Gürdal Z. Design of variable stiffness panels for maximum strength using lamination parameters. Composites B 2011;42(3):546–52.

[48] Ijsselmuiden ST, Abdalla MM, Gürdal Z. Optimization of variable-stiffness panels for maximum buckling load using lamination parameters. AIAA J 2010;48(1):134–43.

[49] IJsselmuiden S, Abdalla M, Gürdal Z. Implementation of strength-based failure criteria in the lamination parameter design space. AIAA J 2008;46(7):1826–34.

[50] Hong Z, Peeters D, Turteltaub S. An enhanced curvature-constrained design method for manufacturable variable stiffness composite laminates. Comput Struct 2020;238:106284.

[51] Hong Z, Peeters D, Guo Y. Efficient strength optimization of variable stiffness laminates using lamination parameters with global failure index. Comput Struct 2022;271:106856.

[52] Guo Y, Serhat G, Gil Pérez M, Knippers J. Maximizing buckling load of elliptical composite cylinders using lamination parameters. Eng Struct 2022;262:114342.

[53] Montemurro M, Catapano A. In: Frediani A, Mohammadi B, Pironneau O, Cipolla V, editors. Variational analysis and aerospace engineering: mathematical challenges for the aerospace of the future. Springer optimization and its applications, 1st ed. vol. 116, (no. 1):Springer International Publishing; 2016, p. 375–400. http://dx.doi.org/10.1007/978-3-319-45680-5.

[54] Montemurro M, Catapano A. On the effective integration of manufacturability constraints within the multi-scale methodology for designing variable angle-tow laminates. Compos Struct 2017;161:145–59.

[55] Montemurro M, Catapano A. A general B-spline surfaces theoretical framework for optimisation of variable angle-tow laminates. Compos Struct 2019;209:561–78.

[56] Catapano A, Montemurro M. Strength optimisation of variable angle-tow composites through a laminate-level failure criterion. J Optim Theory Appl 2020;187(3):683–706.

[57] Fiordilino G, Izzi M, Montemurro M. A general isogeometric polar approach for the optimisation of variable stiffness composites: Application to eigenvalue buckling problems. Mech Mater 2021;153:103574.

[58] Izzi M, Catapano A, Montemurro M. Strength and mass optimisation of variable-stiffness composites in the polar parameters space. Struct Multidiscip Optimisation 2021;64(4):2045–73.

[59] Montemurro M. An extension of the polar method to the first-order shear deformation theory of laminates. Compos Struct 2015;127:328–39.

[60] Montemurro M. Corrigendum to "An extension of the polar method to the first-order shear deformation theory of laminates" [Compos. Struct. 127 (2015) 328-339]. Compos Struct 2015;131:1143–4.

[61] Montemurro M. The polar analysis of the third-order shear deformation theory of laminates. Compos Struct 2015;131:775–89.

[62] Catapano A, Montemurro M. On the correlation between stiffness and strength properties of anisotropic laminates. Mech Adv Mater Struct 2019;26(8):651–60.

[63] Daniel IM, Ishai O. Engineering mechanics of composite materials. Oxford university press New York; 1994.

[64] Vannucci P. A note on the elastic and geometric bounds for composite laminates. J Elasticity 2013;112(2):199–215.

[65] Picchi Scardaoni M, Montemurro M. Convex or non-convex? On the nature of the feasible domain of laminates. Eur J Mech A Solids 2021;85:104112.

[66] Piegl L, Tiller W. In: Springer, editor. The NURBS book. Springer-Verlag; 1997.

[67] Izzi MI, Montemurro M, Catapano A, Pailhès J. A multi-scale two-level optimisation strategy integrating a global/local modelling approach for composite structures. Compos Struct 2020;237:111908.

[68] Nagelsmith M, Guerrits W. Influence of steering radius on the mechanical properties of fiber placed composite laminates. In: ICCS17-17th international conference on composite structures. 2013.

[69] Kraft D. A software package for sequential quadratic programming. Tech. rep., Koln, Germany: DLR German Aerospace Center – Institute for Flight Mechanics; 1988.
[70] Virtanen P, Gommers R, Oliphant TE, Haberland M, Reddy T, Cournapeau D, et al. SciPy 1.0: Fundamental algorithms for scientific computing in python. Nature Methods 2020;17:261–72.
[71] Svanberg K. A class of globally convergent optimization methods based on conservative convex separable approximations. SIAM J Optim 2002;12(2):555–73.
[72] Vannucci P. Plane anisotropy by the polar method. Meccanica 2005;40(4–6):437–54.